CoCO2

Prototype system for a Copernicus CO_2 service

Recommendations on anthropogenic CO_2 emission modelling, evaluation, and optimization

A. Lupascu, A. Agustí-Panareda, J. McNorton, M. Choulga, G. Balsamo, N. Bousserez, M. Guevara, H. Denier van der Gon, K. Politakos, S. Stagakis, N.Chrysoulakis, T. Kaminski, P. Rayner and M. Scholze

Co-ordinated by ECMWF

CoCO2

Prototype system for a Copernicus CO_2 service

D3.2 Recommendations on anthropogenic CO2 emission modelling, evaluation, and optimization

Dissemination Level: Public

Author(s): A. Lupascu, A. Agusti-Panareda, J. McNorton, M. Choulga, G. Balsamo, N. Bousserez (ECMWF), M. Guevara (BSC), H. Denier van der Gon (TNO), K. Politakos, S. Stagakis, N. Chrysoulakis (FORTH), T. Kaminski, P. Rayner (iLab) and M. Scholze (ULund)

Date: 13/11/2023

Version: 1

Contractual Delivery Date: 31/10/2023

Work Package/ Task: WP3/ T3. 2

Document Owner: Organisation

Contributors: ECMWF, BSC, TNO, FORTH, iLab/ULUND

Status: OBJ Final

CoCO2: Prototype system for a Copernicus CO_2 service

Coordination and Support Action (CSA)
H2020-IBA-SPACE-CHE2-2019 Copernicus evolution – Research activities in support of a European operational monitoring support capacity for fossil CO2 emissions

Project Coordinator: Dr Richard Engelen (ECMWF)
Project Start Date: 01/01/2021
Project Duration: 36 months

Published by the CoCO2 Consortium

Contact:
ECMWF, Shinfield Park, Reading, RG2 9AX,
richard.engelen@ecmwf.int

The CoCO2 project has received funding from the European Union's Horizon 2020 research and innovation programme under grant agreement No 958927.

Table of Contents

Figures

Tables

1 Executive Summary

The global CO_2 Monitoring Verification System (CO2MVS) of the Copernicus CO2 Service will use the Integrated Forecasting System (IFS) at ECMWF to estimate global anthropogenic emissions of CO_2 and CH_4. This requires an up-to-date inventory that realistically reproduces the CO_2 anthropogenic emissions, especially in urban areas, where the local contribution from anthropogenic emissions is significant. For this to be modelled it requires a good representation of meteorological processes given that meteorological fields can be used as a proxy for the spatio-temporal distribution of temperature-dependent anthropogenic emissions. Moreover, the spatial representation of large point sources in gridded emission inventories was based on outdated plant level information (Wheeler and Ummel, 2008) and might not be representative of current representation of active power plants.

This report describes the progress of these various aspects during the 33 months of the CoCO2 project. The main results presented here include 1) the extension of IFS code to include the urban canopy model; 2) the use of the best global land cover data set available; 3) development and testing of a heating degree day (HDD) concept that in the end will produce emissions of CO_2 online; 4) testing the implementation of the CoCO2 high-resolution global emission catalogue of CO_2 and co-emitted species (NO_x, SO_2, CO, CH_4) from thermal power plants for the year 2018 developed by Guevara et al. (2023) by using these emissions and associated temporal profiles within IFS. The work on the urban scheme and residential emission model has been published in JAMES (see McNorton et al., 2023). The recommendations for modelling and emissions evaluations include 1) the use of a residential emission model (MEHNDI) coupled with the IFS urban scheme; 2) extending the monitoring network that uses urban eddy covariance flux stations with the final goal of evaluating or optimising high-resolution emission models; 3) the use of point source emissions directly on the IFS grid. For optimization of emissions model parameters, it was recommended that a set of model parameters used by the residential emission model to be optimized with a hybrid ensemble-variational inversion system and the use of the Fossil Fuel Data Assimilation System (FFDAS) either through online or offline integration.

2 Introduction

2.1 Background

In the future European CO_2 Monitoring and Verification Support (CO2MVS) capacity, the estimation of anthropogenic emissions using atmospheric inversion methods relies on the provision of prior information of those emissions as input to the data assimilation system. The prior emission data needs to be as accurate as possible, regarding both its highly variable spatial and temporal distribution. As the statistics used to estimate the emissions in bottom-up global/regional inventories are based on the country and annual scales, proxies need to be used to disaggregate the emissions in time and space (e.g., population, roads, temperature, human settlements, etc.)

In task 3.2 of the CoCO2 project, the aim has been to integrate the emissions that have a clear meteorological forcing and proxy maps that are available within the CO2MVS model. For this reason, the main development has focused on residential heating emissions, which are driven by temperature and urban cover, using the recently implemented urban scheme and tile in the Integrated Forecasting System (McNorton et al., 2021). The approach of heating degree days to represent the variability of residential heating emissions is well known and it has been implemented in many models. Usually, this involves running a heating degree day model offline (e.g., Guevara et al., 2021) with daily mean temperature from re-analyses datasets and then using the resulting daily scaling factors as input to regional and global models. In CoCO2 we have developed an online NWP version of the heating degree day model, which has the

great advantage of providing real-time estimates of the emissions to the global CO2MVS. Moreover, the integration of the urban cover and urban temperature estimation in the IFS will allow the use of high-resolution emissions in the CO2MVS model with as accurate and consistent forcing as possible.

Quantifying the CO_2 emissions of large point sources and cities is one of the main goals of the CO2MVS (Janssens-Maenhout et al., 2020). For this purpose, a high-resolution global emission catalogue of CO_2 and co-emitted species (NO_x, SO_2, CO, CH_4) from thermal power plants for the year 2018 was developed within the framework of CoCO2 (Guevara et al., 2023). We expect the use of this CoCO2 point source emission dataset will improve the representation of the spatial and temporal variability of the thermal power stations in the Integrated Forecasting System (IFS) and the future global CO2MVS.

2.2 Scope of this deliverable

Objectives of this deliverable

This deliverable aims to improve global simulations of CO_2 and to integrate the near-real time CO_2 emissions associated with residential heating as well as an up-to-date power plant emissions catalogue within the IFS system. The objectives are focused on 1) using the urban scheme to improve the near-real time predicted CO_2 residential heating emissions (based on the heating degree day concept) together with the resulting atmospheric CO_2 at urban sites, 2) improving the CO_2 forecast when using emission information for more than 16000 individual facilities defined in the CoCO2 catalogue at their exact geographical location, 3) assess the potential of using eddy covariance flux observations to evaluate the residential heating emission, and 4) provide recommendations for future developments and operational implementation of emission parametrizations in the IFS, as well as the potential to optimise the emission model parameters.

Work performed in this deliverable

- Development of real-time heating degree day model coupled with the urban scheme in the IFS to predict CO_2 emissions from the residential heating sector
- Evaluation of the CO_2 residential heating emissions using flux observations
- Evaluation of the CO_2 residential heating emissions using atmospheric observations
- Use the CoCO2 point source emission dataset for thermal power stations in IFS simulations.
- Provision of recommendations for future global CO2MVS.

Deviations and counter measures

N/A

3 Description of CO_2 emission modelling components for the global CO2MVS

3.1 Urban modelling and the residential heating sector

In recent decades, due to urbanization and rapid economic developments, the consumption of energy has increased, leading to a large amount of carbon emissions. Even though urban environments represent only a small fraction of the global surface, they affect the local climate due to their contribution to urban heat islands. Because of their coarse resolution, most of the global climate models that are utilized for climate change research do not account for urban surfaces (McNorton et al., 2023 and the references herein). The differences between rural and urban coverage should be considered, especially since warming effects associated with the

urban surfaces combined with GHG warming could be important for predicting the changes in mean temperatures. A better understanding of predicted urban temperature is important in assessing the energy consumption or heat- and cold-related mortality. As shown in McNorton et al., 2023, the atmospheric component of the IFS (Integrated Forecasting System) coupled to the land-surface model, ECLand, has been extended to consider the urban tile alongside previously considered land-cover tiles (i.e., surface vegetation, bare soil, snow etc).

As a first step in representing differences between the urban and rural areas in IFS, a single layer-urban canopy model (SLUCM) has been incorporated and will be running operationally in the IFS cycle CY49R1 (2024). This parameterization has previously been assessed in land-surface only and single-column versions of the IFS (McNorton et al., 2021). The purpose of a SLUCM is to provide improved forecast accuracy (e.g., near-surface air temperature and humidity, surface hydrology, energy balance, etc.) for urban environments. A second step was to identify the best global land cover data set for urban cover. For this purpose, the results coming from simulations that used the ECOCLIMAP-SG (Faroux et al., 2013), The Global Human Settlement Layer-S2 (GHSL) (Corbane et al., 2020) and The Copernicus Global Land Cover (CGLC) (Buchhorn et al., 2020) dataset were evaluated against a control simulation which had no urban representation. The simulations ranged from 2018 to 2021 and they were using Tco2556 (~4 km) horizontal resolution with hourly output.

Human activities and activities of biosphere react to changing weather, which leads to temperature-related variability of both emissions and natural carbon cycle. Within the IFS, a weather-dependent online biogenic flux model has been extensively used to simulate atmospheric CO_2 concentrations (Agustí-Panareda, McNorton, et al., 2022; Agustí-Panareda et al., 2019; Boussetta et al., 2013; McNorton et al., 2020). McNorton et al. (2023), extended the heating degree day (HDD) concept, outlined by Quayle and Diaz (1980), which uses atmospheric or surface temperature as a proxy variable for the energy demand for heating buildings and can be used to generate anthropogenic fluxes. The Modelling Emissions from Heating in Near-real-time Driven by the IFS (MEHNDI) system that ultimately generates emissions of CO_2 online was developed and tested within the IFS. The CO_2 emissions used in MEHNDI come from in situ fuel burning for space heating. Other forms of space heating (e.g., electric) were not included since the emissions are often not collocated with heating demands. The main advantages associated with the use of MEHNDI are 1) the improvement of spatio-temporal resolution because of producing fluxes at the resolution of the model; and 2) the availability of near-real-time emissions, which is not the case for inventories based on national reporting. The HDD depends on the temperature, therefore, following Spinoni et al. (2015) a temperature threshold (T_h) of 15.5°C, above which space heating emissions are no longer considered, was considered. As a proxy for daily mean 2m temperature (diagnostic variable within IFS) that is used to calculate the temperature-dependent coefficient, the model soil temperature in the layer (0–7 cm) was used ($T_{soil,1}$). To do so, both diagnostic 2m temperature and soil temperature in layer 1 (0–7 cm) were compared with ERA5 daily mean 2m temperature to determine which variable is most suitable to be used as a varying proxy for daily mean 2 m temperature. The equations are shown below:

$$f(T) = \max(15.5 - T_{soil1}, 1) \qquad (1)$$

$$\gamma = \frac{B}{\sum_0^t \sum_0^x f_{urb,x} f(T_{x,t})} \qquad (2)$$

where B represents 80% of the national residential CO_2 budget (following Guevara et al., 2021) associated with heating emissions (with 20% for non-heating purposes); f_{urb} represents the urban fraction; and t and x spans all times for a given year and all grid cells within the national

domain, respectively. Figure 1 exhibits the heat-depending emissions factor, (γ). The residential sector is then computed with the following equation:

$$F_{CO2,x,t} = f_{urb,x} f(T_{x,y}) \gamma_x \qquad (3)$$

Equation 3 calculates the residential heating emissions at each model time step (alongside all the other meteorological data and online CO_2 fluxes) and at the consistent spatial resolution of the IFS simulation as it is based on a very high-resolution urban cover used to compute the urban fraction f_{urb}. Note the model might fail to represent rural hotspots associated with wood burning as the γ emission factor is nationally constant, which assumes the same method of heating is applied nationally regardless of fuel/technology.

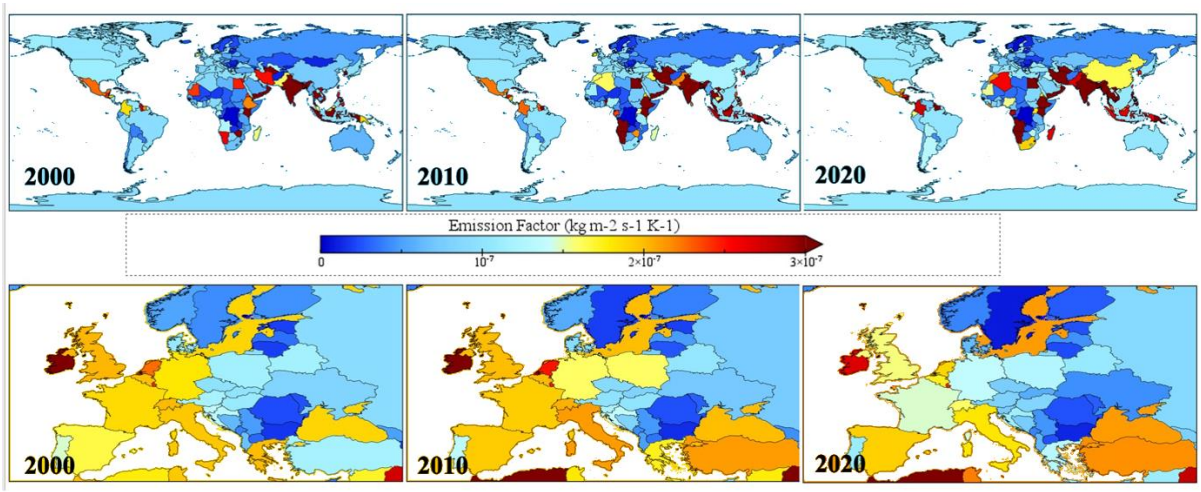

Figure 1 The γ factor depends on the annual country budgets, i.e. it is dependent on technology/activity/people, etc. and therefore, it is not fixed in time time but updated every year from from first soil layer temperature, urban cover and the country-specific CAMS annual budget.

The impact of SLUCM on forecasted meteorological variables together with an assessment of the impact of MEHNDI on predicted CO_2 concentrations will be given in Section 4.

The implementation of MEHNDI with a flexible design, accommodating different input data on different resolutions makes it very flexible regarding the horizontal resolution. As an example,

Figure 2 exhibits a snapshot of the residential emission of CO_2 emissions computed using MEHNDI at a horizontal resolution of 1x1 km for Heraklion, Crete.

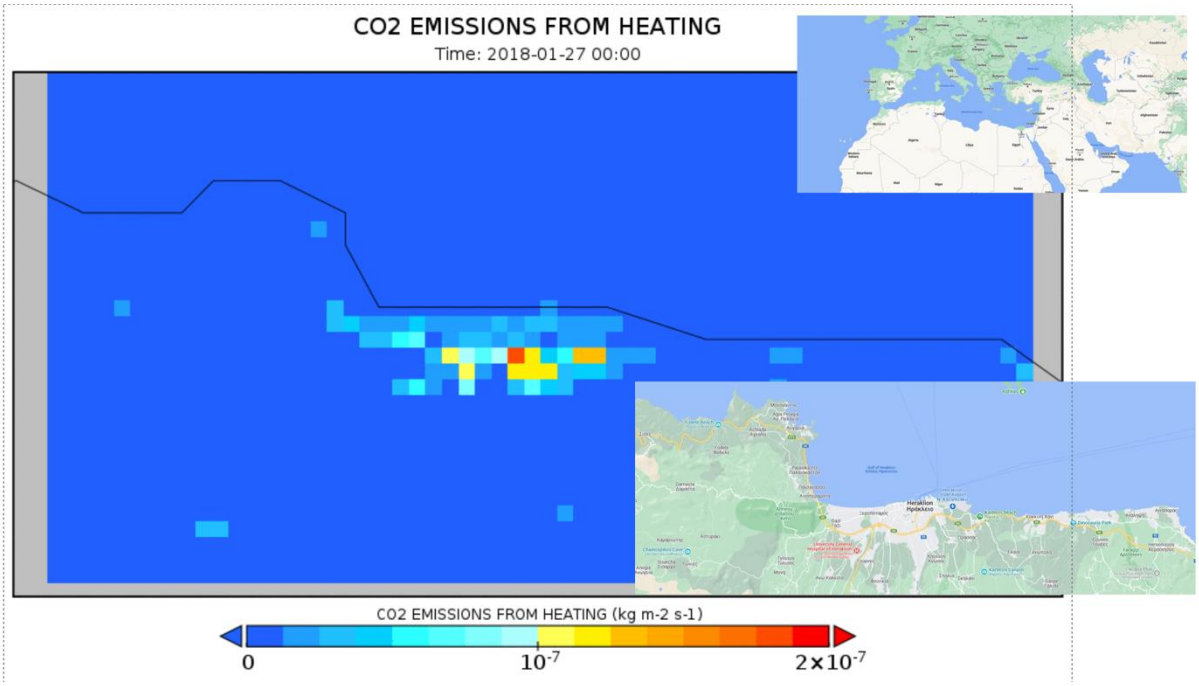

Figure 2 Example of residential heating emissions computed with MEHNDI for the city of Heraklion (Crete) at midnight 27 Jan 2018.

3.2 Point source emissions

Within the framework of the Prototype System for a Copernicus CO_2 service (CoCO2) EU-funded project to support the development of the Copernicus CO_2 Monitoring and Verification Support capacity (CO2MVS) has been developed a high-resolution global emission catalogue of CO_2 and co-emitted species (NO_x, SO_2, CO, CH_4) from thermal power plants for the year 2018. Guevara et al (2023) present in detail how the database has been created, following a bottom-up approach, which combines plant-specific information with national energy consumption statistics and fuel-dependent emission factors and emission ratios. The newly created catalogue contains annual emission information for more than 16000 individual facilities at their exact geographical location. For each power plant, the catalogue contains a specific temporal (i.e., monthly, day-of-the-week and hourly) and vertical distribution profile. Furthermore, the annual emissions presented in the CoCO2 catalogue were compared against independent plant- and country-level inventories, including the Carbon Monitoring for Action (CARMA) and the Emissions Database for Global Atmospheric Research (EDGAR) databases, as well as officially reported emission data. It was noted an overall good agreement between inventories for CO_2 emissions. The main discrepancies are related to the non-inclusion of auto-producer or heat-only facilities in certain countries due to lack of data. However, Guevara et al (2023) indicated that large inconsistencies are obtained when comparing emissions from co-emitted species due to uncertainties in the fuel-dependent emission ratios and gap-filling procedures. They also advise to consider country-dependent temporal profiles when distributing the emissions.

Four simulations were performed: 1) a control simulation that uses monthly emissions from the CAMS-GLOB-ANTv5.3 inventory; 2) a simulation in which the emissions associated with the energy sector in CAMS-GLOB-ANTv5. 3 were replaced by monthly CoCO2 emissions for each facility as in the CoCO2 catalogue; 3) same as 2) but using daily CoCO2 emissions as

derived from the CoCO2 catalogue; 4) same as 2) but using hourly CoCO2 emissions from the CoCO2 catalogue (see also Table 1). For experiments 1) - 3), all gridded emissions files are at 0.1 x 0.1° resolution, for experiment 4) we are using the Tco399 cubic octahedral reduced Gaussian grid.

Table 1 List of experiments performed for 2021

Simulation	Emissions inventory	Emission grid type	Monthly profile	Daily profile	Diurnal profile
ctrl	CAMS-GLOB-ANTv5.3	0.1x0.1°	CAMS-TEMPO (Guevara et al., 2021)	None	Default IFS (Denier van der Gon et al., 2011)
mn	CoCO2 PS	0.1x0.1°	Site-specific CoCO2 PS (Guevara et al., 2023)	None	Default IFS (Denier van der Gon et al., 2011)
dd	CoCO2 PS	0.1x0.1°	Site-specific CoCO2 PS (Guevara et al., 2023)	Site-specific CoCO2 PS (Guevara et al., 2023)	Default IFS (Denier van der Gon et al., 2011)
hr	CoCO2 PS	Tco399	Site-specific CoCO2 PS (Guevara et al., 2023)	Site-specific CoCO2 PS (Guevara et al., 2023)	CoCO2 PS (Guevara et al., 2023)

We also analyse the impact of emissions resolution using daily CoCO2 PS emission on 0.1x0.1° grid and on the Tco399 cubic octahedral reduced Gaussian grid.

4 Evaluation

4.1 Urban temperature and winds from IFS

To assess the model's skill in simulating observed meteorology when the SLUCM is employed, and to find out which land cover leads to best results, the modelled 2m temperature and 10m wind speed were evaluated against SYNOPs database (McNorton et al., 2023). Given that the majority of the ~6000 sites are in non-urban areas and that urban land cover in the IFS represents only 0.3% of total land cover, the impact of SLUCM is not expected to be important, yet the use of this scheme overall reduces the RMSE values for the 2 m temperature by ~0.5% and for wind speed by 0.65%–0.94%. 27 urban SYNOP sites were used to evaluate the direct contribution of the urban scheme.

When the SLUCM scheme was employed, the negative bias of 2m temperature seen in the IFS control experiment was reduced for all urban SYNOP sites, except Istanbul, Delhi and Sydney (see Figure 3).

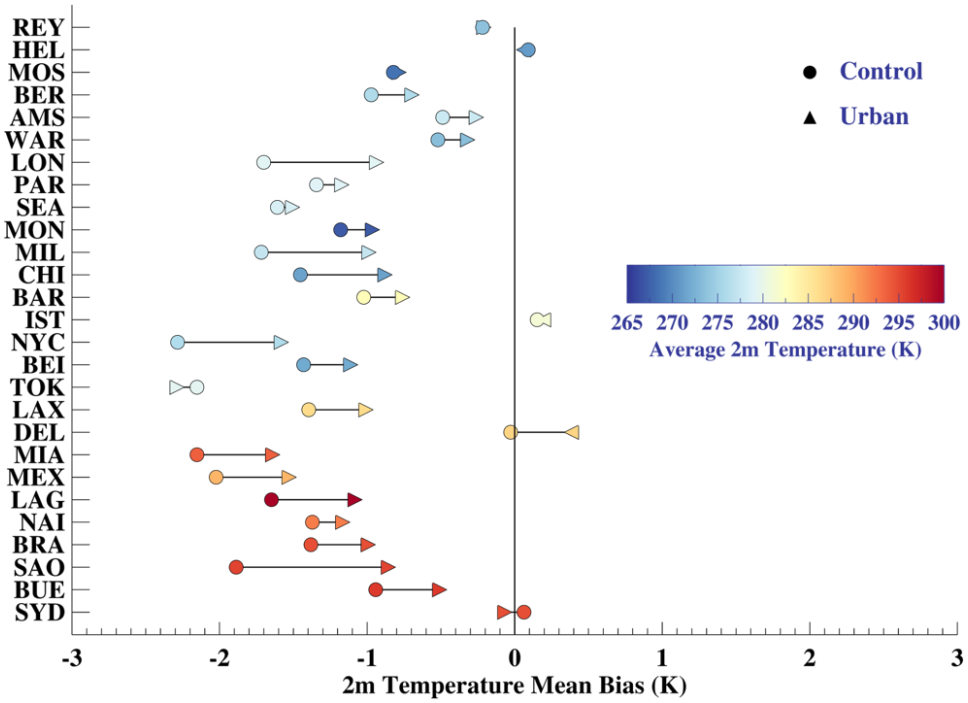

Figure 3 The 2 m temperature mean bias for the urban IFS (IFS_U, triangles) and control IFS (IFS_C, circles) compared with 27 urban SYNOP sites for DJF 2018. The color represents the average observed temperature for the city for the specific season.

Furthermore, as shown by McNorton et al (2023), the selected urban SYNOP sites were divided between the airport and non-airport sites for 10 m wind evaluation (Figure 4). IFS urban simulation reduces the wind speed, bringing down the mean bias for all SYNOP sites characterized as non-airport from +0.53 ± 1.10 to −0.26 ± 1.33 m s −1. Over airport sites, the low bias associated with the IFS control simulations (DJF: −0.21 ± 1.13 m s −1, JJA: −0.28 ± 1.20 m s −1) was further decreased when SLUCM scheme was employed (DJF: −0.71 ± 1.08 m s −1, JJA: −0.76 ± 1.18 m s −1). This behaviour can be linked to the poorly represented roughness length for momentum since it is used as a simplistic model approach whereby urban environments have a fixed road-to-building ratio of 0.5 and building height of 8 m for all grid cells. In reality, airport sites should have a much higher road-to-building ratio.

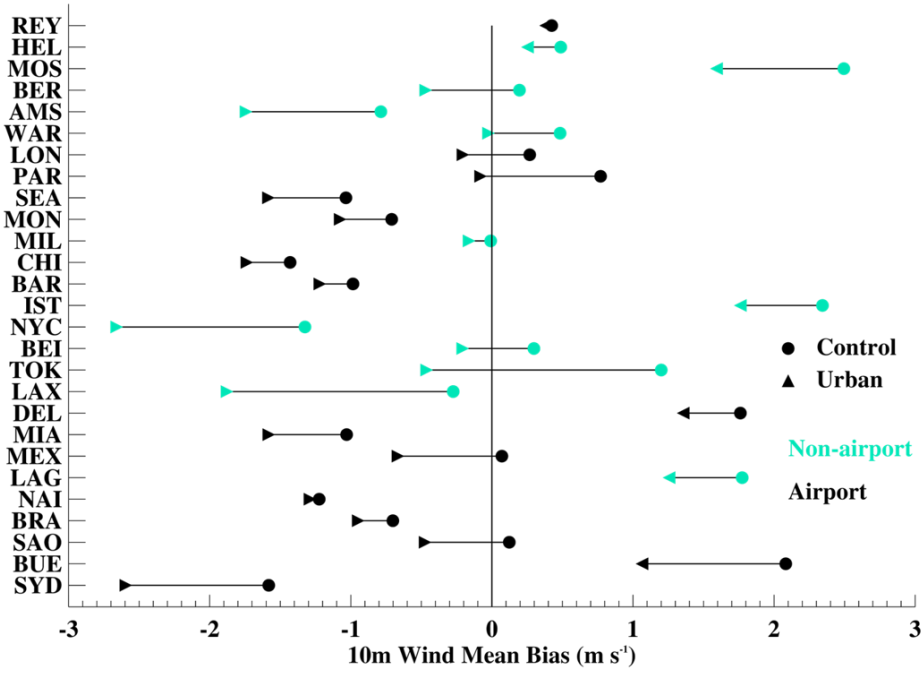

Figure 4 The 10 m horizontal mean bias for the urban IFS (IFS_U, triangles) and control IFS (IFS_C, circles) compared with 27 urban SYNOP sites for DJF 2018. The color differentiates between airport and non-airport sites.

In a nutshell, McNorton et al (2023) showed that the implementation of the urban scheme in IFS improved 2 m temperature (~10%) and 10 m wind (~17%) RMSE values for both summer and winter months around urban environments. The influence of the scheme was most noticeable at night.

4.2 Using flux observations to evaluate residential heating emission model

Flux Observations in Heraklion (local scale)

Eddy covariance (EC) is the only direct measurement technique of vertical heat and mass transfer (fluxes) between the Earth's surface and the atmosphere at large spatial scales. EC is based on the simultaneous measurement of gas concentrations (or temperature) and 3D wind velocities at high frequency (usually 10 or 20 Hz) on tall or medium size towers, depending on the morphology of the surface structures. EC has been established as the standard measurement technique of surface GHG fluxes over several ecosystem types, such as forests, grasslands, or crops, and is used worldwide to monitor ecosystem behaviour and responses to climate change and anthropogenic disturbances since a couple of decades.

Collaborative entities, national organizations, scientific institutes, and universities have orchestrated substantial scientific forums and initiatives to amass EC datasets. In Europe, a notable example of such efforts is the Integrated Carbon Observation System (ICOS, https://www.icos-cp.eu/) and the European Fluxes Database Cluster (http://gaia.agraria.unitus.it/). On a global scale, one of the most densely distributed networks, encompassing a multitude of these initiatives, is FLUXNET, achieving a truly worldwide reach, with measurement sites spanning every continent. FLUXNET is dedicated to the provision of EC flux measurements in carbon, water vapour, and energy exchange, thereby contributing significantly to our understanding of Earth's ecosystems (https://fluxnet.org/).

More recently, the EC method has been applied to urban environments (Aubinet et al., 2012), providing a wealth of results for a variety of urban centers with different building types, land use, morphology, climate, population distribution, and geographic extent. In this context, FORTH operates two ICOS Associated urban flux towers in Heraklion area, Crete (https://rslab.gr/fluxtowers.html), so that accurate estimates of the city's emissions can be obtained for representative parts of the city. One in a residential area Mastambas (hereinafter: HECMAS) and a second one in the city center of Heraklion (hereinafter: HECKOR), Crete, established in April 2021 and in November 2016 respectively (Figure 5). Both flux towers are equipped with IRGASONs (Integrated CO_2/H_2O Open-Path Gas Analysers and 3D Sonic Anemometers) and net radiometers (online real-time measurements: https://rslab.gr/heraklion_eddy.html). These measurements can contribute to the formulation of local policy-making to tackle climate change, by keeping the relevant authorities constantly informed on the progress of urban emission mitigation. Furthermore, through FORTH's research activity, Heraklion is already included in European-scale CO_2 emission monitoring studies (Nicolini et al., 2022) and also in global research (Lipson et al., 2022).

In an urban area, the EC measuring instruments are placed above the average building height so that the airflow is not obstructed, and the measurements are representative of a large area of the underlying urban surface upwind, called flux footprint. Computation of the area of footprint within urban spaces may facilitate the recognition of crucial emission sources and differentiation between various urban covers with distinct emission properties such as building heating, commuting or traffic. The extent of the footprint area can be determined by analytic algorithms taking into account the wind direction and speed and the roughness of the urban surface (Kljun et al., 2015).

Figure 5 FORTH's flux towers, as they operate until today, HECKOR (on the left - commercial area, Heraklion's city center) and HECMAS (on the right - residential area).

Local urban CO_2 flux measurements are affected by different emission sources and sinks. The observed flux (F_c) between the urban surface and the atmosphere can be decomposed to the main urban flux components as follows (Figure 6):

$$F_c = E_V + E_B + R_H + R_S + (R_V - P_V) \qquad (4)$$

Where, E_V stands for emissions from cars, E_B for emissions from buildings, R_H for respiration from people and animals, R_S for soil respiration, R_V for above-ground plant respiration, and P_V for the uptake of CO_2 by plant canopies through photosynthesis. The positive sign indicates direction towards the atmosphere (net emissions) and the negative sign towards the surface (net uptake) (Ben Crawford et al., 2011; Moriwaki & Kanda, 2004; Stagakis et al., 2019).

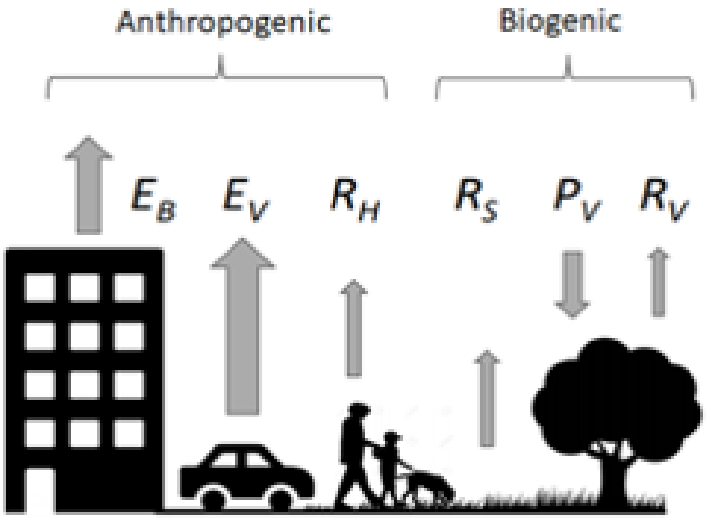

Figure 6 Local scale CO_2 flux (Fc) components within urban areas.

How to use observations in the comparison with modelled fluxes

The assessment of the modelled space heating emissions by MEHNDI using the local urban EC observations is a challenging task. The following steps are suggested:

4.2.1.1 EC flux processing and quality control

The first step would be to process the EC datasets and perform a robust quality control and gap-filling procedure to obtain reliable and continuous flux time series. This approach entails multiple steps that include a thorough examination of all measurements prior to the processing phase. To begin, diagnostic flags are assigned by default to each high-frequency measurement from both the gas analyser and sonic anemometer, which are used to reject any reading of inferior quality. In addition, each measurement is followed by signal strength diagnostics, which are used to determine the operational state of the instruments. To improve data integrity, the raw dataset is de-spiked and filtered while adhering to preset maximum and minimum data thresholds. Moreover, quality flags are produced for every 30-minute interval in the flux data, based on the results of both steady-state testing and evaluations of turbulent conditions. (Stagakis et al., 2019).

F_C measurements lost by the above procedure are gap-filled using the method introduced by Schmutz et al. (2016). A moving LUT (mLUT) technique is implemented that fills F_C gaps according to wind direction (± 25º), time of day (± 1.5 h) and day (± 4) through an iterative process that chooses the temporally closest F_C value that meets the wind direction criterion. Sundays are treated separately in the mLUT technique due to their unique emission patterns, considering only this type of day in the day criterion (± 3 Sundays). After the application of this method, the loss of F_C measurements in our dataset is drastically reduced.

4.2.1.2 EC flux footprint estimation

The second step would be to model the EC flux footprint and compare it to the model resolution. If the extents can be comparable, then the evaluation of the modelled data can provide meaningful insights. To achieve this goal, the technique leverages the Flux Footprint Parametrization (FFP) model developed by Kljun et al. (2015). The FFP model is a crucial tool for assessing the local geographical region which contributes to the observed fluxes. The collection of two basic types of information is required for the estimation of a dynamic flux footprint. To begin, static data contains a complete Digital Surface Model (DSM) that defines the surface characteristics surrounding the flux tower, including building structures and trees. Furthermore, the general topography of the surrounding region is described using a digital terrain model (DTM). Second, the dynamic component of the data is the collected micrometeorology by the EC system. The anisotropic morphology and roughness estimations of 400 m radius around each tower are linked with the 30-min meteorological forcing data from the EC according to the wind direction. Thus, roughness length (z_o) and displacement height (z_d) are variable according to wind direction in correspondence to the urban morphology. Kljun et al. (2015) define the measurement height (z_m) as the height above displacement height ($z_m = z_{receptor} - z_d$). z_o is directly used as an input parameter to FFP. The rest of the FFP inputs are the standard deviation of lateral velocity fluctuations, wind direction, friction velocity (u^*), Obukhov length (L) and planetary boundary layer height (PBLH). Wind attributes, u^* and L were calculated from the EC measurements for each 30-minute period. PBLH is estimated for each 30 m period combining (Zilitinkevich et al., 2012) and (Nieuwstadt, 1981) diagnostic formulas for neutral and stable conditions and Batchvarova and Gryning (1991) simplified turbulence kinetic energy equation for convective conditions. The Monin-Obukhov stability parameter (z_m/L) is used for the indication of atmospheric stability regime. More specifically, Zilitinkevich et al. (2012) and Nieuwstadt (1981) diagnostic formulas were used to give the initial height during night-time stable and neutral conditions and then (Batchvarova & Gryning, 1991) equation was used to determine the rate of change of PBLH for each 30-min period during the convective daytime conditions.

The computation of flux footprints was done in Heraklion to determine the long-term turbulent flux source area, as shown in Figure 7). The 30-minute footprints produced from all valid EC measurements made during the course of the research period's 12-month period were aggregated. Consequently, the FFP follows wind pattern, regarding Heraklion in an annual basis, the predominant wind directions are mostly from the North (N) to the Northwest (NW) and from the South (S) to the Southwest (SW).

The original spatial resolution of MEHNDI covers a much larger area than the measurements represented by the flux tower footprint. Consequently, any correlation conducted without consideration would yield inaccuracies. To avoid this, ECMWF provided specifically, for Heraklion, Greece and Basel, Switzerland, MEHNDI products with downscaled output of ~1km^2 at a daily time-step for the years 2018, 2021 and 2022.

4.2.1.3 Source/sink analysis or attribution

As described in Section 4.2.1, the urban EC flux measurements are affected by several sources and sinks. Quantifying the different components within the measurements (source attribution) is challenging. There are some approaches suggested in the literature (e.g. B. Crawford & Christen, 2015; Stagakis et al., 2019) but can be very site-dependent and based on various assumptions. Overall, there are still no robust methods to quantify the different CO_2 flux components measured by an urban EC station at short time scales (hourly to daily).

Nevertheless, there are several types of analyses that can help understanding the source/sink patterns of each urban EC site and at least qualitatively describe the main flux components contributing to the observations. The simplest approach is to group the flux datasets according

to wind direction, season, and day of the week (weekday-weekend). Comparison of the daily flux patterns between the different groups can provide insights of the main contributing components. A more detailed analysis involves the footprint estimations linked to a land cover/use map of the site. Such analysis can provide footprint weighted contributions of the different land cover types to the measured fluxes (e.g. Stagakis et al., 2019). Different land cover types can be associated to various sources or sinks and therefore the method can provide quantitative estimations of the contributing flux components. Even though this method is promising, it still relies on several assumptions and cannot be very precise.

Footprint weighting can also be applied to flux model outputs if the model resolution permits (e.g. Stagakis et al., 2023). Such approach can help in the comparison between models and observations if all contributing components are modelled. If the model resolution is much lower than the footprint extent or if not, all flux components are modelled, the comparison would involve certain assumptions.

4.2.1.4 Scaling and units

Models and observations may “talk different language.” One has to make sure that the comparisons make sense in terms of the sectoral, spatial, and temporal allocation of the modelled fluxes compared to the observations. The unit scales can also be a source of discrepancy. EC observations are usually expressed as mass per m^2 of footprint area per unit of time. Modelled emissions are expressed kg m^{-2} s^{-1}. Appropriate scaling has to be applied if the modelled emissions are not expressed in the same units or in case of quite different reference areas (footprint vs grid cell) in terms of land cover type fractions.

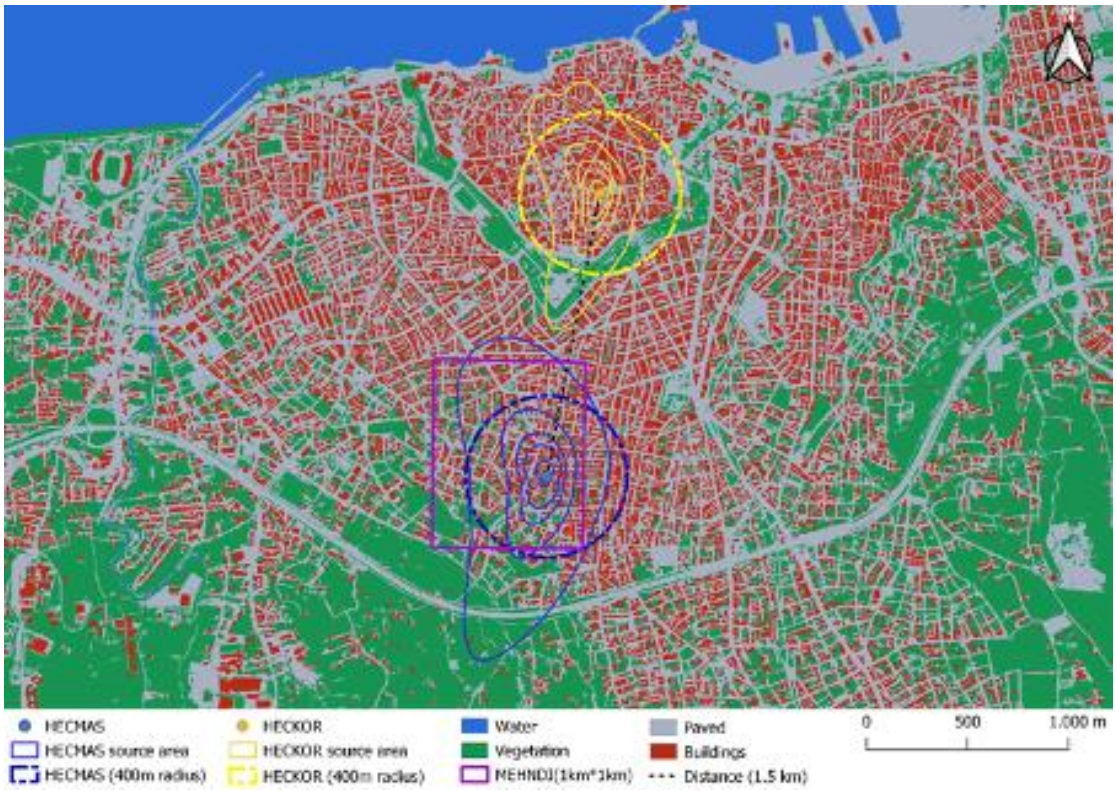

Figure 7 Land cover map of Heraklion. The blue and yellow contours represent average turbulent flux source areas isopleths (1 year) of HECMAS and HECKOR, respectively. Each MEHNDI grid box (~1 km^2) represents distinct areas. For the current analysis, only the purple grid box located within the flux footprint area of HECMAS from the MEHNDI dataset was used.

Correlation of the in-situ Eddy Covariance measurements with MEHNDI heating emissions product

Among, the four flux tower sites, two in Basel and two in Heraklion, we had to determine which areas were most affected by heating emissions throughout a typical year characterized by mild summers and cold winters. HECKOR exhibits distinct features, primary business areas and major thoroughfares (in an annual basis ~70% of the total F_C is derived from traffic accumulation (Stagakis et al., 2019)), serving both commercial and commuter purposes (Politakos et al., 2023a). The emissions from the flux towers located in Basel, would also not be ideal as they both observe fluxes from major roads and commercial/industrial buildings (Stagakis et al., 2023). HECMAS is primarily characterized by residential neighborhoods featuring high building density and limited, sparse vegetation areas. Small stores and a limited number of public facilities, including schools, complement the surrounding neighborhood. The annual CO_2 fluxes in this region are primarily influenced by heating emissions, particularly during the colder months when heating demands are higher. The traffic network is typified by intersections with low to moderate traffic activity. The northern, more distant part of the region showcases a higher density of low vegetation, including grass and crops (Politakos et al., 2023). Therefore, in our analysis, we chose only HECMAS station which is affected majorly by building heating emissions and only minorly by the rest of the urban sources or sinks.

Our analysis drew upon observations spanning from December 2021 to April 2022. This period aligns with the noticeable decline in temperatures in Heraklion, which commenced in December and rose gradually in March, a trend corroborated by HECMAS observations and MEHNDI simulations. The MEHNDI grid cell that overlaps with the flux footprint was selected for the correlation as shown in Figure 8. MEHNDI heating emissions were normalized by urban fractions variables, provided by ECMWF.

On top of Figure 8, the daily CO_2 heating emissions calculated using the MEHNDI grid cell model (orange line) over the HECMAS observations (blue line) are presented. Throughout the entire year, HECMAS observations reveal a consistent pattern wherein F_c remains consistently low during the warm months and rises significantly during the cold months. It is worth noting that the MEHNDI calculations align closely with the Heating Degree Days (HDD) calculations outlined in Section 4.1. Consequently, a minimum constant value during the warm period of the year (June 2021 – November 2021 and April 2022 – May 2022) is observed when the daily temperature measurements in Heraklion exceed the HDD lower threshold of 15.5° Celsius, as specified by the European Centre for Medium-Range Weather Forecasts (ECMWF). Conversely, the EC observations exhibit a distinct weekly pattern during the warm months. This weekly pattern is intricately tied to the behaviour of residents and commuters. The observations reveal that Saturdays and Sundays exhibit low Fc values, reflecting the closure of most stores and public services, resulting in fewer cars on the road. The first peak in emissions occurs at the start of the week on Monday, reaching its climax on Wednesdays when a flea market is held regularly. Subsequently, emissions decrease towards the end of the workweek.

During the cold period, spanning from December 2021 to the end of March 2022, both MEHNDI emissions and EC observations show an increase. For MEHNDI, this signifies that the daily HDD values correspond to lower temperatures in Heraklion, consistently below 15.5° Celsius threshold. The EC observations reveal a pattern, characterized by localized peaks and not a distinct weekly consumption pattern seen earlier in the year. Additionally, the consistent behavior of residents throughout the cold period contributes to lower values that still exist in the background even if they are not still distinguished due to the higher impact of the heating emissions. In summary, it can be inferred that the higher values in observed emissions correspond to the heating needs of residents, thereby establishing a stronger correlation between HECMAS and MEHNDI. However, it is essential to acknowledge that MEHNDI presents lower emissions due to its sectorial approach, focusing solely on heating emissions. Conversely, EC observations encompass a broader spectrum, considering the

covariance in the local urban atmosphere, including sources and sinks from the footprints, including vehicle emissions, respiration, and heating emissions.

We calculated monthly means for both results and then performed a linear fit correlation analysis to catch the impact of these peaks in the model and observations, focusing on the cold period. The two bar plots exhibit consistent monthly patterns, succinctly illustrating that lower temperatures lead to higher values in MEHNDI heating emissions, which also has a direct and immediate impact on the EC observations. Upon conducting a linear fit analysis, the results were exceptionally good, with an R-squared value of approximately 96%, and a p-value of 0.004 indicating a strong and positive correlation.

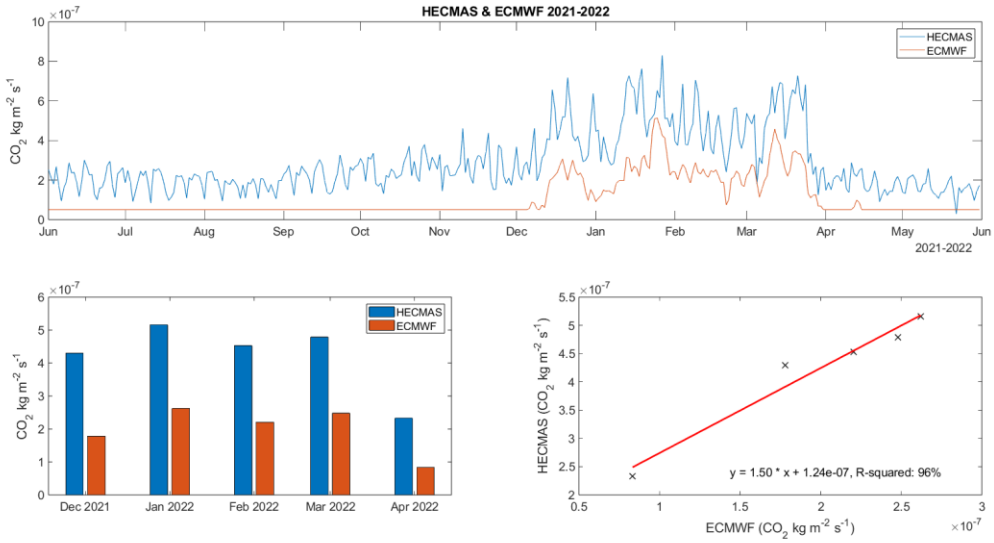

Figure 8 The top plot shows daily mean FC from EC measurements (HECMAS, blue) and CO_2 heating emissions (MEHNDI, orange). The bottom left graph presents monthly means of both variables (during the cold months), and the bottom right plot shows a linear regression model fit of the monthly aggregated variables.

Caveats

Section 4.2, although was not initially from the primary objectives of this deliverable, the collaborative efforts between FORTH and ECMWF during CoCO2 project, brought initiatives for exploration and progress of the project. Among this process, a few caveats have been detected, that could be useful in future versions of the model, beyond the CoCO2 but also of broader initiatives (i.e., CORSO).

Primarily, the process of downscaling a global model into ~1 km^2 grid pixels for conducting evaluations within the flux footprint area, was a unique process for MEHNDI's typical outputs. As previously mentioned, EC measurements can effectively characterize the exchanges in energy and mass within the flux footprint area, but it is challenging to extract forcing data at ~1km^2, in such high-resolution data, particularly when applied to extensive geographic regions. This is a limitation that could be achieved and evaluated, particularly through initiatives CO2MVS, providing direct observations with greater spatiotemporal resolution.

Certainly, up to this point, MEHNDI has primarily focused on describing heating emissions; this is why correlations were conducted for HECMAS during a specific period, among three other flux towers' observations. To enhance its capabilities, would be advantageous to include additional components from Equation 4. For instance, R_H, could be calculated utilizing human activities and population density grids, which are already available in the literature with

increased spatio-temporal resolution. Expanding the analysis in this manner could yield more comprehensive results, potentially leveraging networks like FLUXNET or ICOS to conduct broader and more extensive evaluations. Moreover, by then MEHNDI could play a pivotal role in drawing up strategies and informing policymakers, offers realistic values from a global, regional or even a neighbourhood scale.

4.3 Impact of residential heating emission model on atmospheric CO_2

Emissions of CO_2 produced by MEHNDI were first evaluated against the existing CAMS residential emissions (Granier et al., 2019), which provide monthly grid scale estimates of emissions (CAMS), and the CAMS TEMPO-ral profiles (TEMPO), which provide daily rescaling based on an offline HDD approach (Guevara et al., 2021).

There are several differences between TEMPO and MEHNDI. First, TEMPO rescales the existing inventory based on the spatial distribution provided by the CAMS inventory whereas MEHNDI generates emissions based on the spatial distribution of the urban scheme introduced here. Second, TEMPO uses ERA5 daily mean 2m temperature, which is not available in real-time, whereas MEHNDI uses the first layer soil temperature, available at model resolution, as a proxy for daily mean temperature. Third, TEMPO ensures the annual budget is conserved by averaging a scaling factor across all days to 1, which is also not possible in near-real-time simulations, whereas MEHNDI scales the emission factor map by extrapolating budgets from previous years. This results in slight differences between the annual budgets, for example, 2020 annual global CAMS and TEMPO emissions (3.48 Pg CO_2) are slightly larger than MEHNDI (3.39 Pg CO_2). Finally, we have introduced a maximum HDD value of 15.5, assuming for temperatures below 0°C residential emissions no longer continue to increase from heating. This simple assumption is based on an assumed heating capacity, but will either be removed or refined in future developments. These four differences between TEMPO and MEHNDI explain the difference in derived emissions from several countries shown in Figure 9. The daily variability, driven by temperature changes was apparent in both MEHNDI and TEMPO at the national scale, when compared with CAMS. This variability was larger for TEMPO, which is expected given daily average of 2 m temperature varies with greater magnitude and on timescales slightly shorter than the first soil layer, used by MEHNDI. MEHNDI emissions from high-latitude regions were stable over winter months, relative to TEMPO, caused by the minimum temperature threshold at which emissions increase being set to 0°C. For the temperate regions there was typically a good agreement between MEHNDI and TEMPO. The spatial difference in emissions showed changes introduced by using the land cover map from the urban scheme, we focused on emissions from Western Europe for a given day (9 January 2020) as an example case (Figure 10).

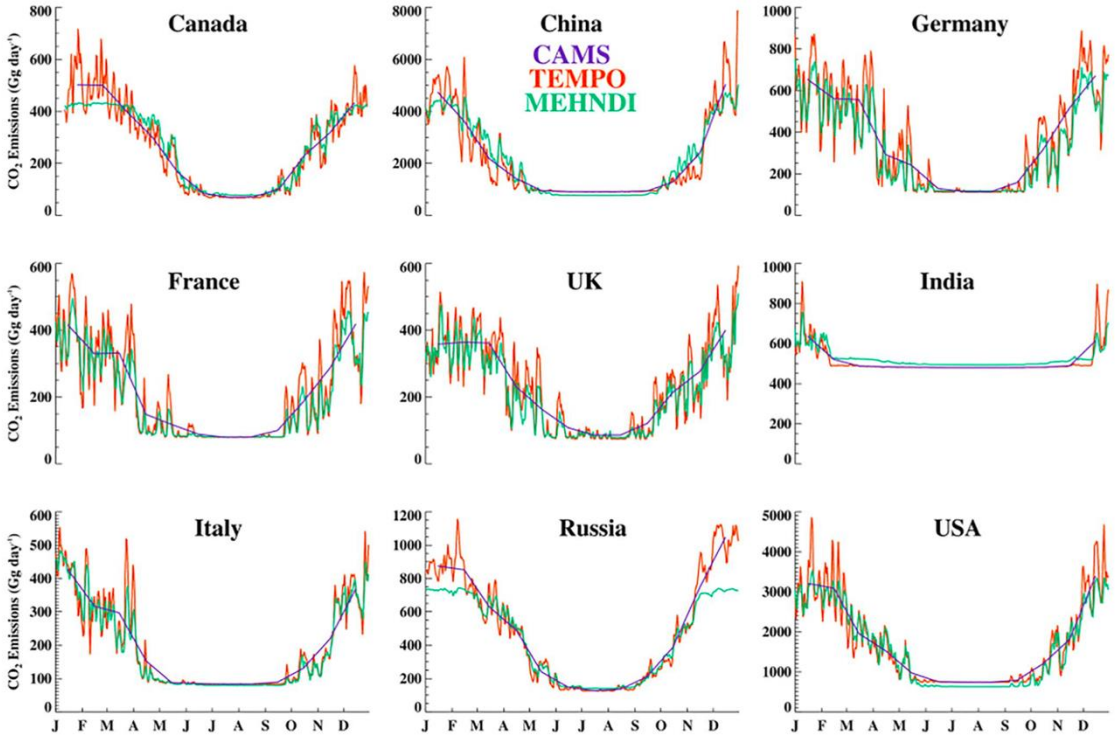

Figure 9 National residential sector emissions of CO_2 for 2020 from the CAMS inventory (monthly, purple), TEMPO (daily, red) and MEHNDI (daily, green) for nine countries.

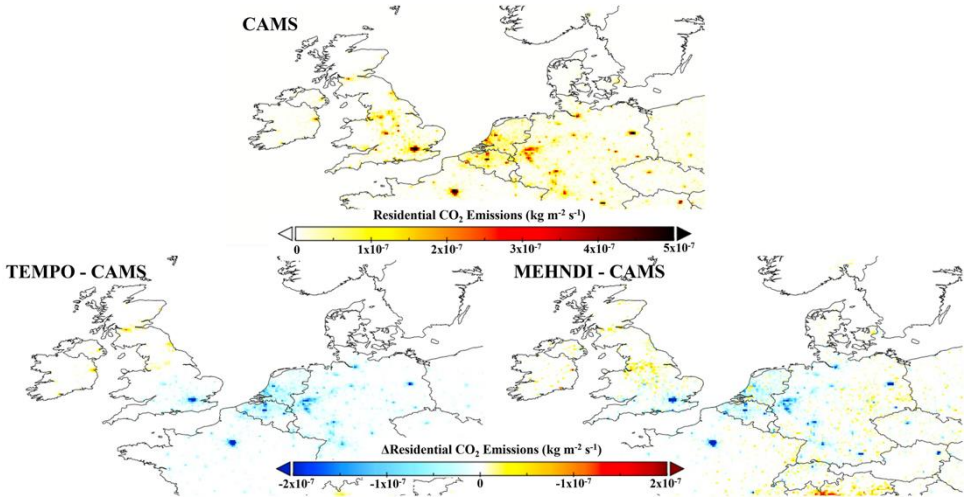

Figure 10 Spatial distribution of residential sector emissions from the CAMS inventory for 9 January 2020 (top). The difference between TEMPO and CAMS emissions for the same date (bottom left). The difference between MEHNDI and CAMS emissions for the same date (bottom right)

The TEMPO and MEHNDI emission estimates for 2020 were compared with daily domestic natural gas consumption data for France provided by the natural gas transmission system operator, GRTgaz (GRTgaz, 2022). The consumption is measured at all delivery points connected to the public distribution network and, it is assumed, should strongly correlate with residential CO_2 fluxes. Comparisons show good agreement with both TEMPO (R = 0.95) and MEHNDI (R = 0.97), suggesting both emission data sets provide an accurate representation of the daily variability in residential CO_2 emissions at the national scale (Figure 11). Variability

between weekdays and weekends was evident in summer months in the gas consumption data which is not present in either emission data set. Implementation of societal habits beyond temperature comfort would be required to simulate this. Weekly profiles of residential emissions, used by the LOTOS-EUROS model (Denier van der Gon et al., 2011), could be incorporated into the system as a first step; however, these would only be representative of Europe. The temperature threshold, linear increase in gas consumption with decreasing temperature and 80% of gas used for heating assumptions are evaluated using the same data and show the modelled consumption is accurate (Figure 11). As previously noted, this is a reasonable assumption for France and is not ideal for all countries.

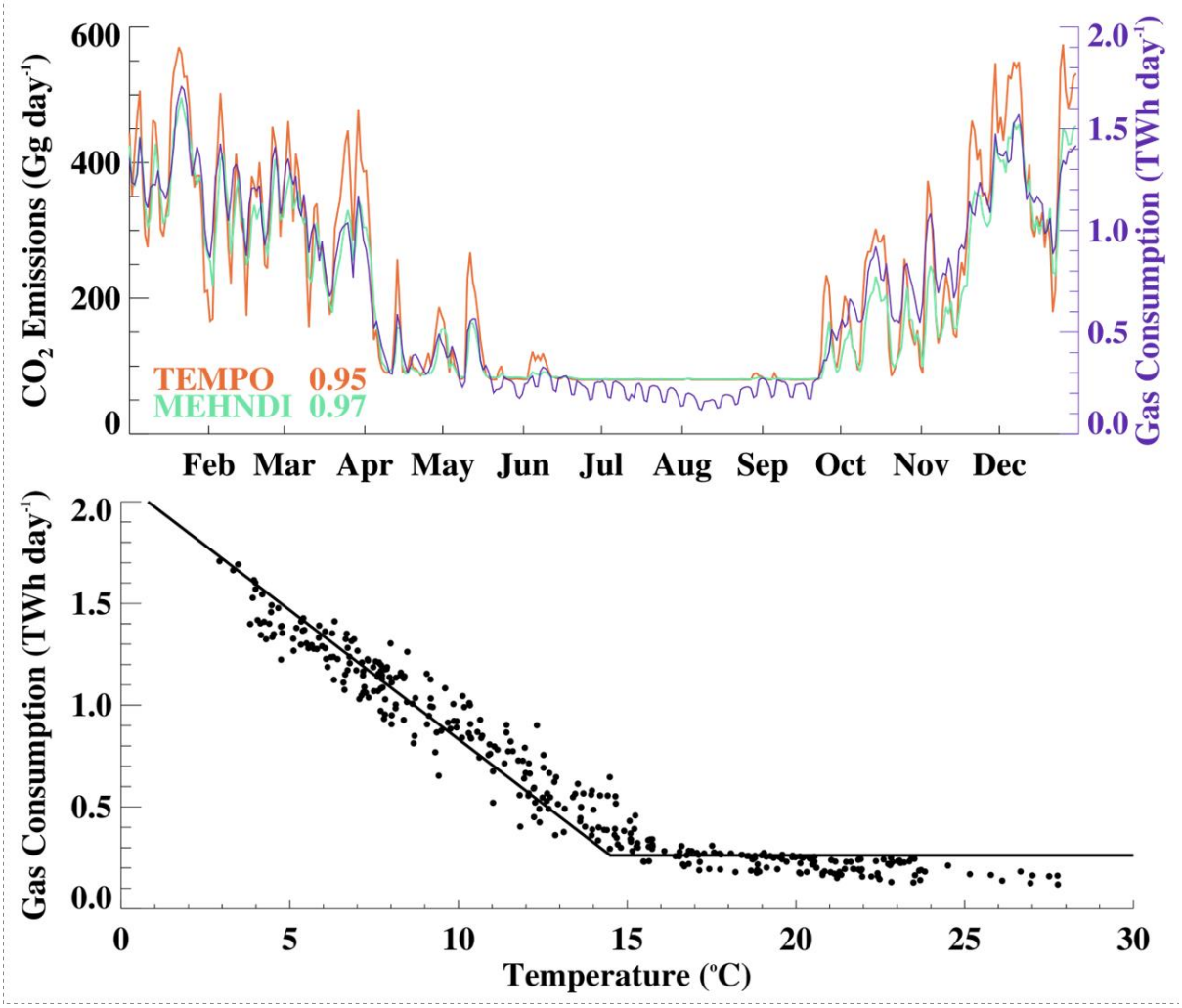

Figure 11 Daily CO_2 emissions from the residential sector for 2020 from TEMPO (left-axis, red) and MEHNDI (left-axis, green) from France (Top). The daily domestic natural gas consumption data for France from GRTgaz (right-axis, purple). Also shown are the Pearson correlation coefficients for both emission inventories compared with GRTgaz data. The daily domestic natural gas consumption against the IFS first soil layer daily urban national average temperature over France for 2020 (Bottom). The line indicates the modeled consumption based on a linear function of temperature, a temperature threshold of 15.5°C and assuming 80% of consumed gas is for heating.

To evaluate the atmospheric impact of emissions from MEHNDI several sensitivity experiments were performed using the CAMS operational system for 2020 (IFS_CAMS, IFS_MEHNDI, IFS_TEMPO). The setup mirrored the NWP setup previously described including the horizontal resolution (~9 km), which is higher than the Tco399 (~25 km) used by the operational CAMS forecast (Agustí-Panareda et al., 2019). All non-residential fluxes used are taken from the CAMS inventory described by Agusti-Panareda, Barré, et al. (2022) or use the online biogenic flux model described by Boussetta et al. (2013). Atmospheric CO_2 concentration fields were output at 3-hourly intervals and 137 vertical levels. The residential sector's contribution to total global CO_2 fluxes was small, however for certain times at local scales, the impact of using the different emissions was observable in the total column CO_2 concentrations (XCO_2) with differences of up to 4 ppm (Figure 12).

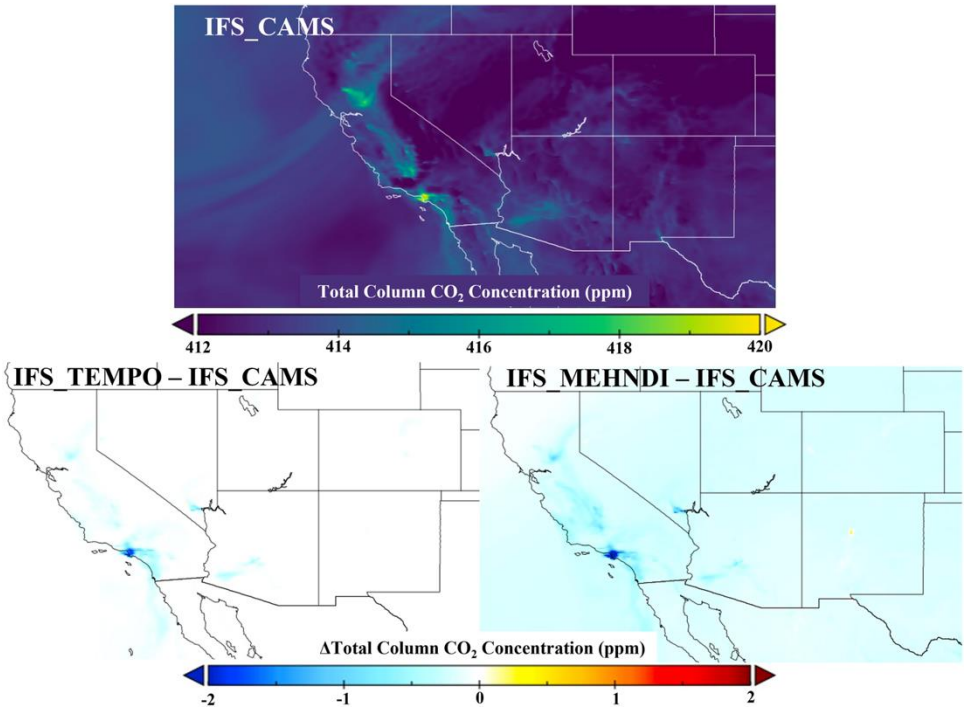

Figure 12 IFS total column CO_2 (XCO_2) over western USA using the CAMS residential sector emissions at 18:00 UTC, 2 February 2020 (top). The difference in XCO_2 between the IFS using CAMS-TEMPO and the IFS using CAMS emissions for the same time and region (bottom left). The difference in XCO_2 between the IFS using MEHNDI and the IFS using CAMS emissions for the same time and region (bottom right).

The Total Column Carbon Observing Network (TCCON) provides XCO_2 observations from multiple sites with a high accuracy (Wunch et al., 2011). Sounding-specific TCCON averaging kernels were applied to model fields for model–observation comparisons as described in Massart et al. (2016). We focused on TCCON sites near large urban conurbations, where the XCO_2 signal is likely to be strongly influenced by local residential sector emissions. The six selected sites were Karlsruhe, Germany (Hase et al., 2014), Nicosia, Cyprus (Petri et al., 2019), Paris, France (Té et al., 2014), Pasadena, USA (Wennberg et al., 2014), Reunion, France (De Mazière et al., 2014) and Saga, Japan (Kawakami et al., 2014). As previously noted, residential emissions make up only a small fraction of the total anthropogenic emissions, and therefore an even smaller fraction of the total CO_2 emissions. Therefore, as expected, the impact of the different emissions on XCO_2 concentrations was small, even close to urban hotspots (Figure 13). Despite this, simulations which use daily fluxes provided a more accurate representation of XCO_2 at all 6 sites. IFS_MEHNDI produces the lowest RMSE at all

sites and the highest r *v*alue at five out of six sites. A key factor is that the overall budget is lower in the MEHNDI inventory, as it is not constrained by the nationally reported figures. This reduces the total atmospheric burden, which considering the model XCO_2 is typically high bisas relative to TCCON, can explain some of the improvement. However, the improvement is not as considerable at other background TCCON sites, and the correlation improvement does not account for this reduction in bias. This would suggest MEHNDI provides an improved spatiotemporal disaggregation of emissions relative to the existing inventory.

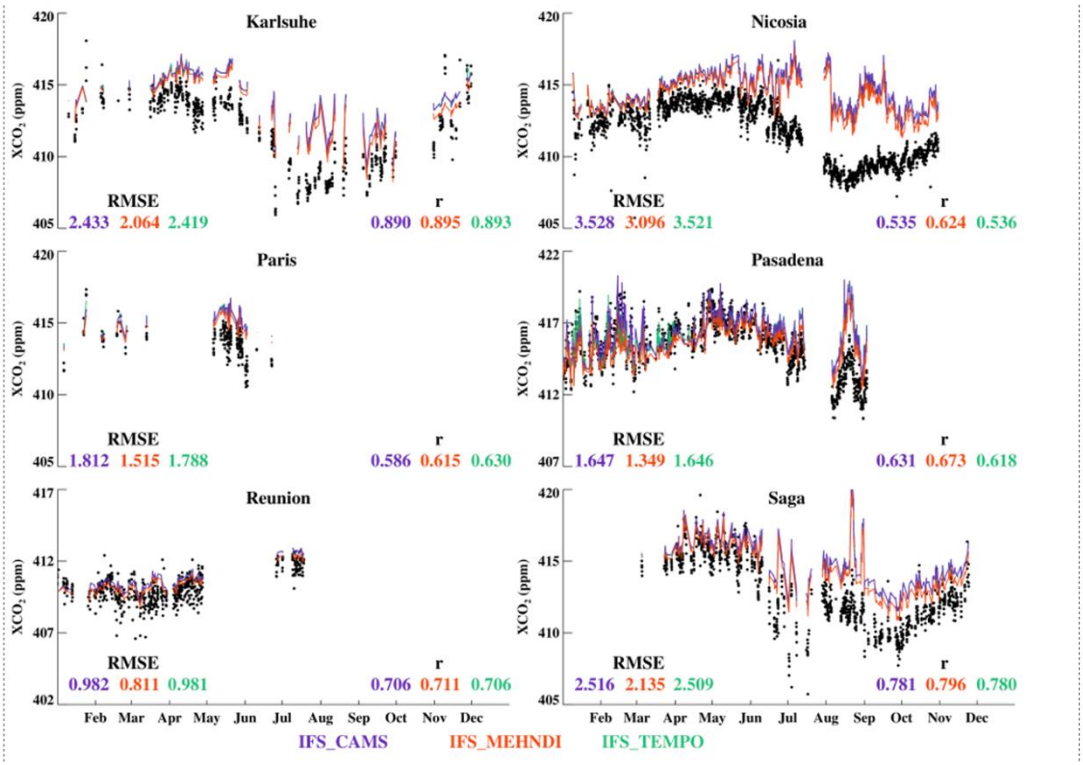

Figure 13 IFS total column CO_2 (XCO_2) and TCCON retrievals over six sites for 2020. Simulations consist of three different residential emissions (IFS_CAMS—purple, IFS_MEHNDI—green and IFS_TEMPO—red) all with the TCCON averaging kernel applied. Values given are RMSE and Pearson correlation (r) compared to TCCON retrievals. Note that often IFS_TEMPO values are very close to IFS_CAMS.

4.4 Plume simulations from power stations

In this section, we investigate the variability in CO_2 and XCO_2 concentration levels when using emissions for the energy sector from the CAMS-GLOB-ANTv5.3 (Soulie et al, 2023) and CoCO2 PS (Guevara et al., 2023) inventories. We will also analyse the impact of the CoCO2 temporal profiles (monthly, daily, hourly) on predicted surface and total column CO_2. We focus on a case study at the Matimba power station (South Africa) that has been misallocated in the EDGARv5 and CAMS-GLOB-ANTv5.3 emission datasets. The total estimated CO_2 emissions for South Africa from the energy sector are 238.069 and 224.744Tg/yr in the CAMS-GLOB-ANTv5.3 and CoCO2 PS inventories respectively. This suggests that Matimba was included as an important source of CO_2 emissions in the CAMS-GLOB-ANTv5.3 but misallocated in the grid.

Figure 14 (upper panel) exhibits the monthly variation of the CO_2 emission fluxes associated with the power sector at Matimba. We note that the CO_2 emissions from CAMS-GLOB-

ANTv5.3 are within 3 factors of magnitude lower than those coming from the CoCO2 PS inventory due to the geographical misallocation in the CAMS-GLOB-ANTv5.3 inventory. Moreover, we also note that the monthly emissions differ when using different approaches to construct the input emissions files from the CoCO2 PS inventory. As mentioned in Section 3.2, the hourly emission files are written directly on the Tco399 grid, and not interpolated onto the reduced Gaussian grid. The spatial remapping from the regular grid to the reduced Gaussian grid uses a box-average interpolation as a proxy for conservative remapping. Due to the relatively coarse resolution of the domain (25 km) when compared with the input emission data (~10 km), the remapping leads to a smoothed emission distribution (see also Fig S1). Therefore, the remapping performed using a nearest-destination-to-source approach performed directly on the IFS grid results in a ~28% increase in the emissions fluxes at Matimba.

Figure 14 (bottom panel) illustrates the plant-level emissions flux when combining the information on monthly emissions with the fixed hourly temporal profiles per sector and the temporal profiles reported in the CoCO2 catalogue. We note that the fixed hourly variation profiles clearly differentiate between the night- and daytime and display a morning peak, while the reported CoCO2 profile does not show this large variation, and it peaks in the afternoon.

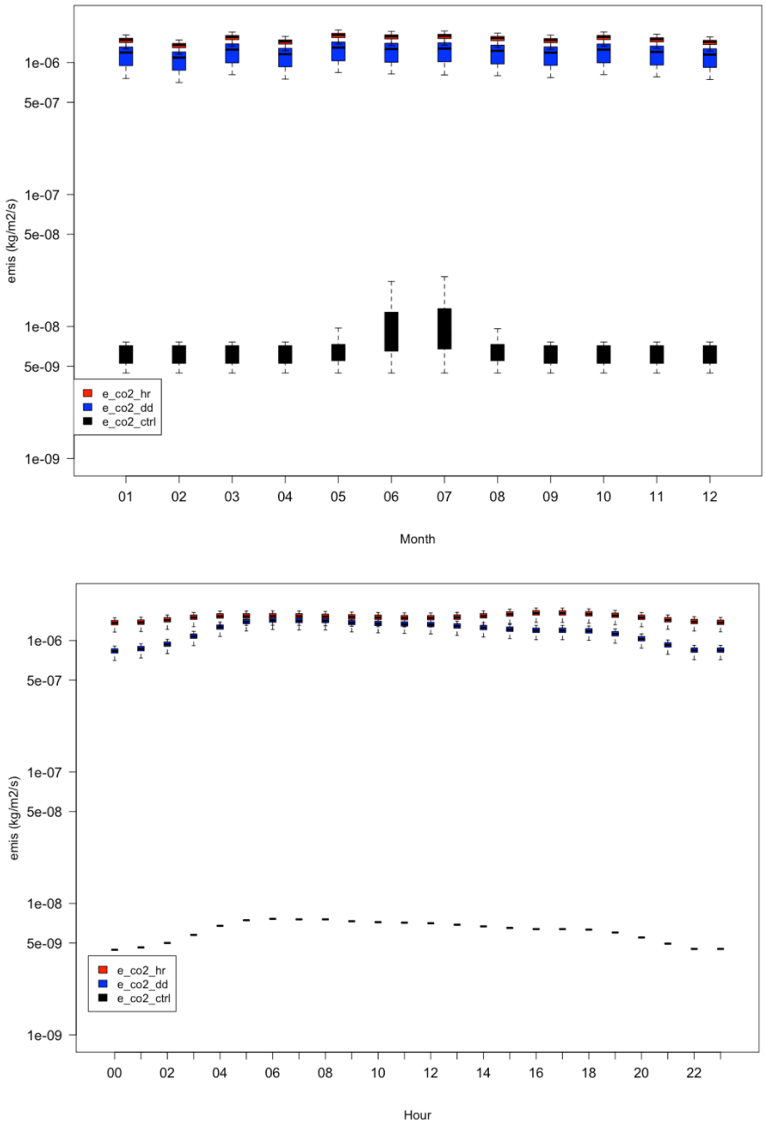

Figure 14. Monthly (upper panel) and hourly (lower panel) variation of the CO_2 emissions from the power sector at Matimba. The CAMS-GLOB-ANTv5.3 emissions are in black, CoCO2 PS daily emissions are in blue, and CoCO2 hourly emissions are in red. The line in the middle of each box is the mean, while the boxes represent the 5th and 95th percentiles.

The spatial pattern of XCO_2 is presented using 11 July 2021 mean values as an example in Figure 15. Concentrations calculated with the CoCO2 PS run are significantly higher than those from CAMS-GLOB-ANTv5.3 in the grid cells situated at the border between South Africa and Botswana. In addition, the use of the CoCO2 PS emissions leads to an increased XCO_2 concentration at/near the Matimba power station. This is more visible on the plots in the lower panel that depict the difference between the various CoCO2 PS simulations and the control run. From those plots, it is clear that Matimba is missing in the CAMS-GLOB-ANTv5.3 emission inventory, and the emissions are relocated elsewhere. This leads to a dipole in the difference between CAMS-GLOB-ANT and the CoCO2 PS inventories. Since the daily and diurnal variability is averaged over the whole month, the general spatial pattern in monthly concentration is similar.

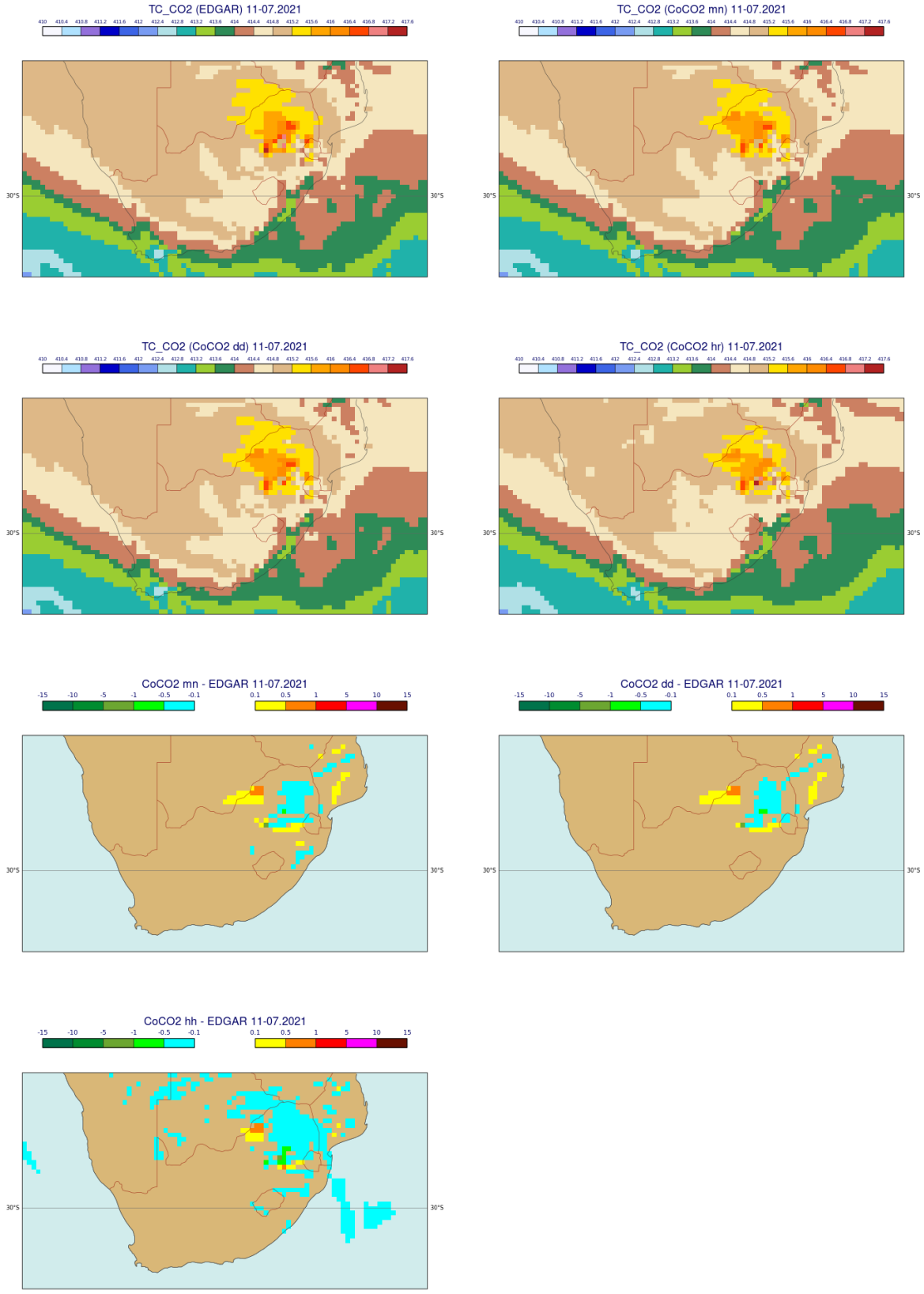

Figure 15 Average XCO_2 for all experiments and difference between simulation using the CoCO2 PS emissions and control experiment for 11 July 2021

The use of CoCO2 PS inventory leads to an increase in predicted surface and total column CO_2 concentration (Fig. 16) compared to CAMS-GLOB-ANTv5.3, highlighting the uncertainties in the gridded emission inventory. The effect of site-specific diurnal profiles has no impact on surface concentration, mostly because of the assumption that the emissions are equally distributed in the model layers ranging from 200 to 800m. The XCO_2 concentration has a similar diurnal variation when using monthly and daily CoCO2 emissions, however, we note a different behaviour when a site-specific diurnal profile is applied, with a small underestimation of XCO_2 compared to the simulations that are using the standard diurnal profiles. The use of a site-specific diurnal profile has no impact on monthly mean XCO_2 in the first part of 2021 and tends to predict slightly less XCO_2 in the second part of 2021. In the following, we examine the impacts on CO_2 and XCO_2 concentrations of different spatial and temporal allocations of the emissions for January 2021.

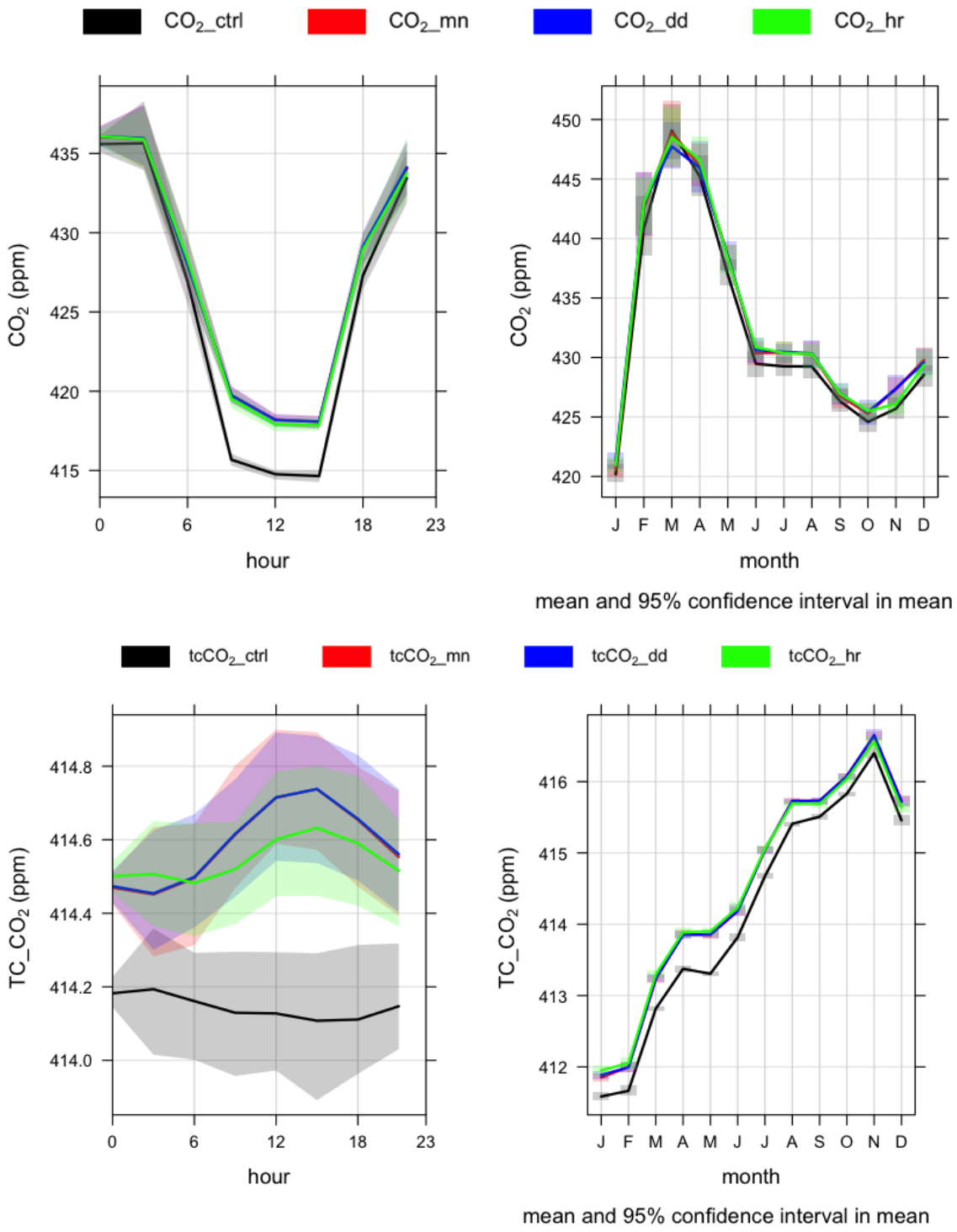

Figure 16 Time variation of predicted surface CO_2 (upper panels) and XCO_2 (lower panels) concentration at the Matimba power station (South Africa). The lines indicate the concentration from the use of CAMS-GLOB-ANTv5.3 with the standard diurnal profile (black), CoCO2 PS using monthly emissions with the standard diurnal profile (red), CoCO2 PS using daily emissions with the standard diurnal profile (blue) on a regular grid and CoCO2 PS using hourly emissions with site-specific diurnal profile (green) on the Tco399 grid.

To disentangle between the combined effect of emissions input files being written directly on the IFS grid and the use of different diurnal profiles, we compare against the observations the predicted CO_2 and XCO_2 from simulations for January 2021 that are using 1) daily CoCO2 PS emission on 0.1x0.1° grid with standard diurnal profile (further named dd_nc); 2) daily CoCO2

emissions on Tco399 cubic octahedral reduced Gaussian grid with standard diurnal profile (further named dd_gr) and 3) hourly CoCO2 emissions on Tco399 cubic octahedral reduced Gaussian grid with site-specific diurnal profile (further named hh_gr). Due to their remote location, the TCCON stations are not strongly affected by the emissions from power plants. Yet the model bias (Figure 17 and Table 2) shows, generally, a slight improvement when comparing the results from the dd_gr and hh_gr simulations with those from dd_nc, highlighting the role of better spatial allocation when we use directly the Tco399 grid. As noted by Guevara et al. (2023), the CoCO2 PS catalogue does not include emissions from non-European auto-producer facilities in several countries due to the lack of information, and the countries affected by this limitation are Russia, India and Japan, where the share of national emissions that could not be assigned to individual facilities for these countries is between 14% and 21%. The CO_2 emission budget in Japan is 365.14 and 219.83 Tg/yr in CAMS-GLOB-ANTv5.3 and CoCO2 PS, respectively, and this might explain why at the Saga and Tsukuba sites, the use of CAMS-GLOB-ANTv5.3 leads to higher XCO_2 concentrations. Overall, we note slight differences between the XCO_2 simulations from dd_gr and hh_gr when we allocate the emissions on the same grid but using different diurnal profiles. This can be explained by the local nature of the emission differences and the rapid mixing in the atmosphere, as noted by Lian et al (2021).

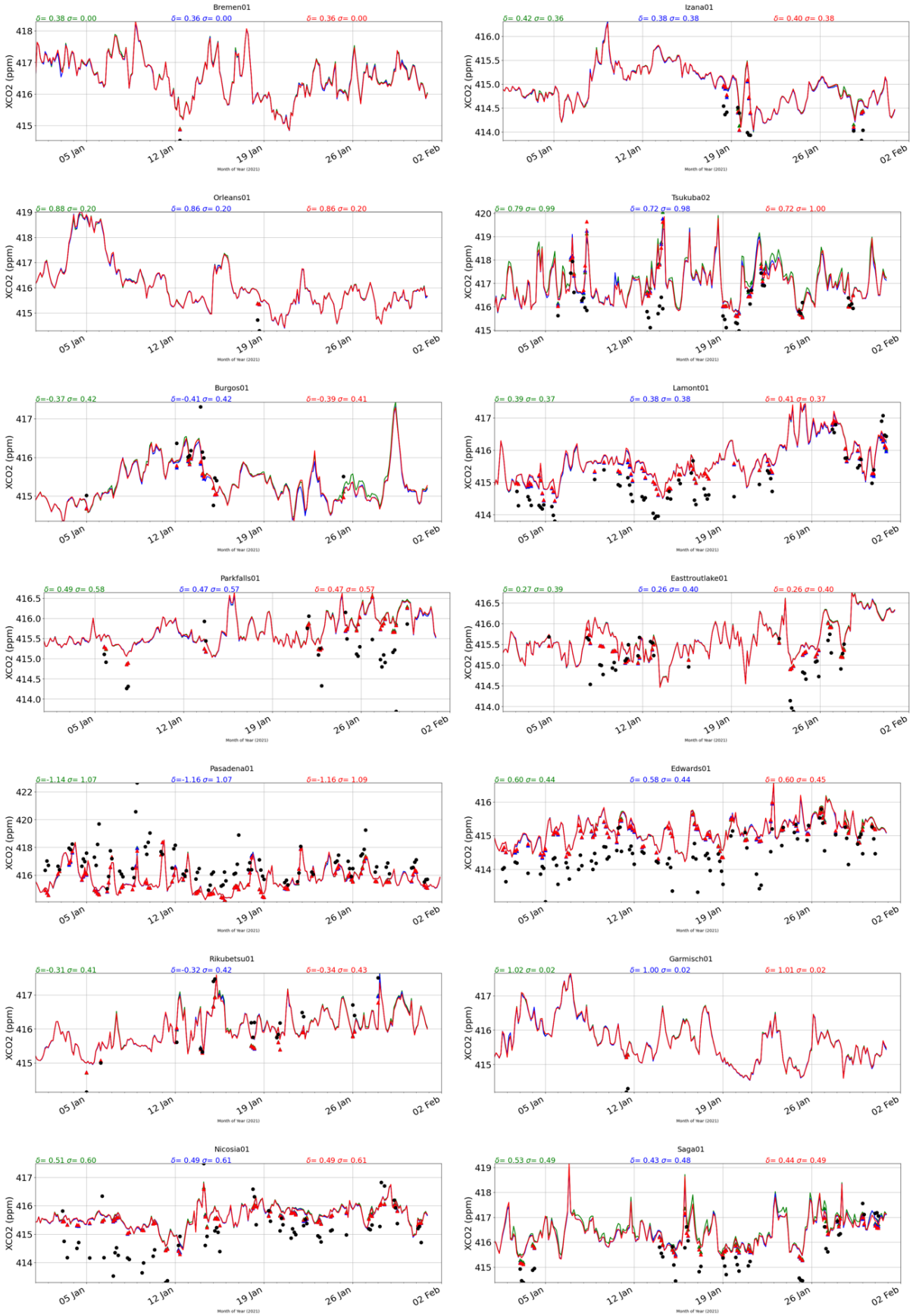

Figure 17 Time series of 3-hourly observed (black dots) and modelled XCO_2 from the dd_nc (green), dd_gr (blue) and hh_gr (red line) for January 2021

Table 2 Observed mean and simulation summary statistics for XCO_2. The bias, and root mean square error (RMSE) are calculated between simulated and observed XCO_2 at TCCON sites during the 1–31 January 2021 period.

Station	Obs mean	Model mean			bias			RMSE		
		dd_nc	dd_gr	hh_gr	dd_nc	dd_gr	hh_gr	dd_nc	dd_gr	hh_gr
pasadena	416.81	415.67	415.65	415.65	-1.14	-1.16	-1.16	1.56	1.58	1.59
bremen	414.53	414.91	414.88	414.89	0.38	0.36	0.36	0.38	0.36	0.36
burgos	415.85	415.47	415.44	415.46	-0.37	-0.41	-0.39	0.56	0.59	0.57
edwards	414.44	415.04	415.02	415.03	0.6	0.58	0.6	0.75	0.73	0.75
East troutlake	415.09	415.37	415.36	415.36	0.27	0.26	0.26	0.48	0.47	0.48
garmisch	414.25	415.27	415.25	415.25	1.02	1	1.01	1.02	1	1.01
izana	414.18	414.6	414.56	414.58	0.42	0.38	0.4	0.55	0.53	0.55
lamont	414.96	415.35	415.35	415.37	0.39	0.38	0.41	0.54	0.54	0.55
orleans	414.51	415.38	415.37	415.37	0.88	0.86	0.86	0.9	0.88	0.88
parkfalls	415.15	415.64	415.62	415.63	0.49	0.47	0.47	0.76	0.74	0.74
rikubetsu	416.1	415.78	415.77	415.76	-0.31	-0.32	-0.34	0.51	0.53	0.54
saga	415.57	416.1	416.01	416.01	0.53	0.43	0.44	0.72	0.65	0.65
tsukuba	416.1	416.88	416.82	416.82	0.79	0.72	0.72	1.26	1.22	1.23
wollongong	411.9	411.96	411.93	411.93	0.06	0.03	0.03	0.84	0.83	0.81
nicosia	415.03	415.54	415.51	415.52	0.51	0.49	0.49	0.79	0.78	0.78

Similarly, the impact of gridded spatial resolution and diurnal profile on predicted surface concentration can be seen in Fig 18 and Table 3. We note that different spatial and temporal allocation has an impact on surface sites located in the proximity of cities, such as Boston University (bu) near Boston, MA, USA, and Egbert (egb) near Toronto, ON, Canada. Although the impact is relatively small, we expect it will be much larger when running the IFS model at higher resolutions (e.g. operational resolution of 9 km and higher resolution used in DestinE project of ~4.5 km). As can be seen in Figure S2, the remapping from the regular grid to Tco399 leads to the smoothing of emission fluxes near Egbert, ON, Canada, and to a different spatial allocation of the emissions. The atmospheric flow near Egbert has a strong north-westerly component, thus the site was located upwind of the pollution source, explaining close biases between the dd_gr and dd_nc simulations. The temporal profile from the CoCO2 PS catalogue is somehow constant throughout the day when compared with the standard temporal profile (not shown). Thus hh_gr has larger emissions during the nighttime compared with dd_gr. This leads to more CO_2 confined at the ground level during the nighttime in Toronto, that, after the break-up of the stable nocturnal boundary layer, could be transported further downwind, explaining the higher bias calculated at Egbert in hh_gr compared to that in dd_gr (Table 3).

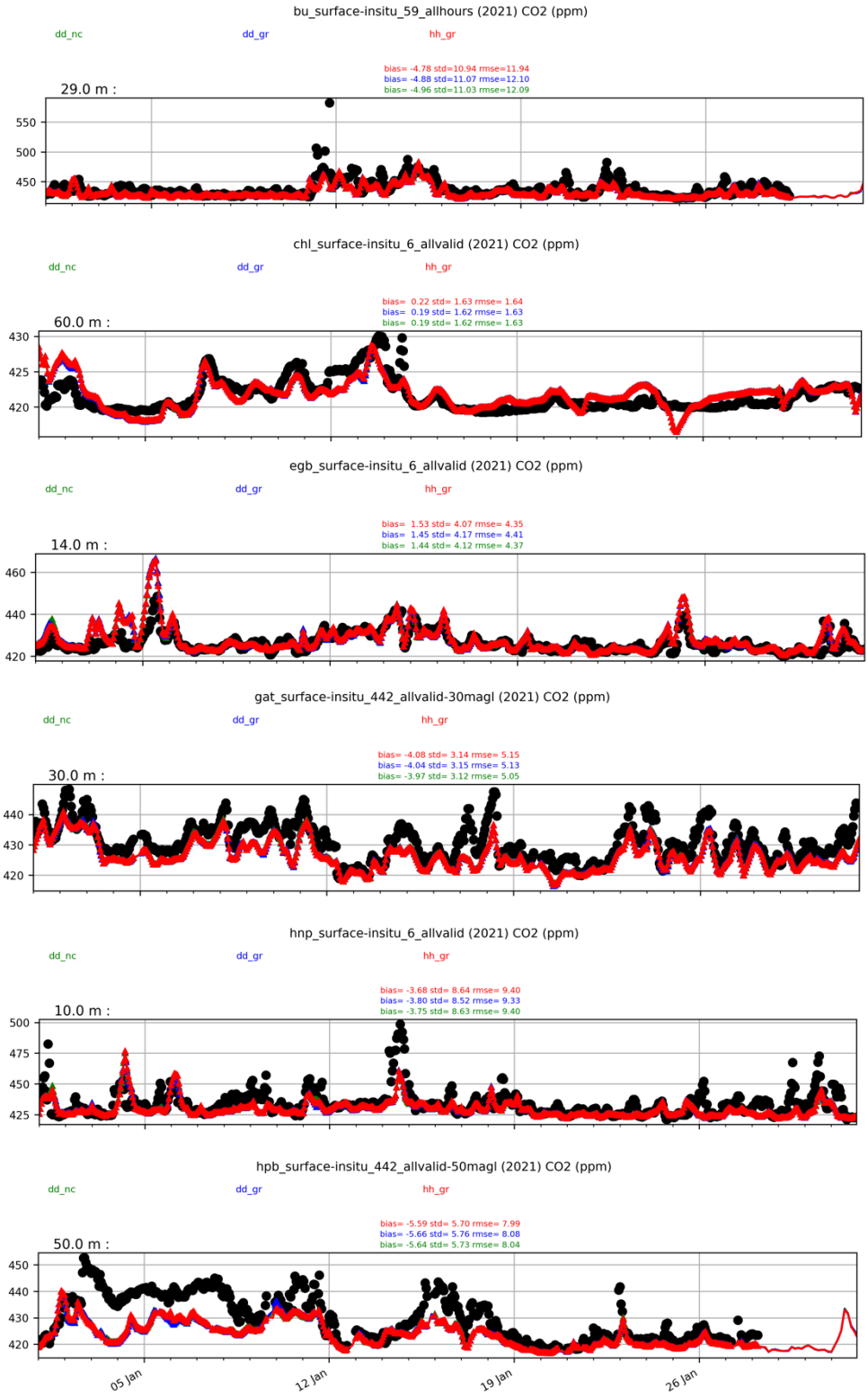

Figure 18 Time series of 3-hourly observed (black dots) and modelled CO_2 from the dd_nc (green), dd_gr (blue) and hh_gr (red line) for January 2021

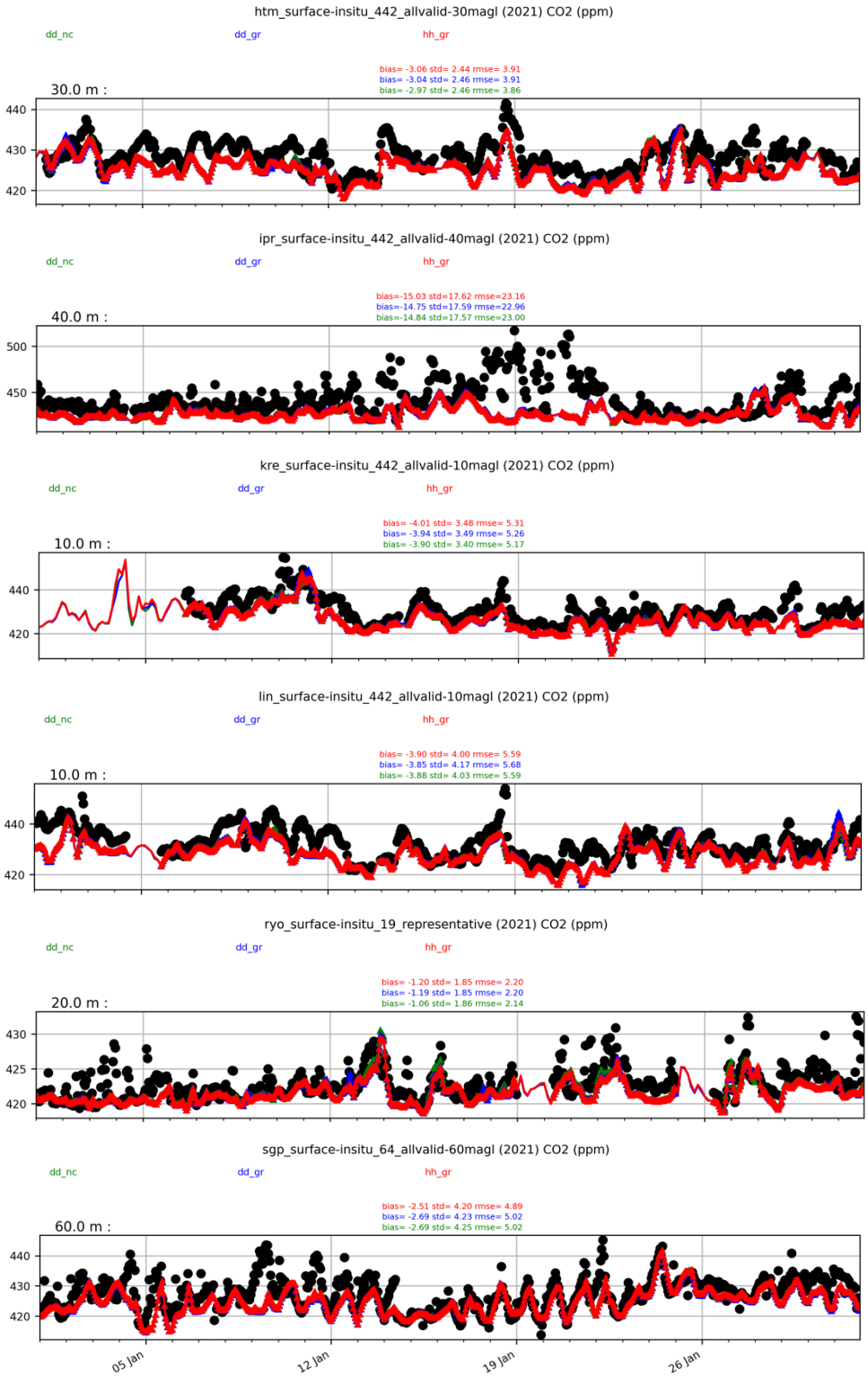

Figure 18. Cont

Table 3 Observed mean and simulation summary statistics for CO_2. The bias, and root mean square error (RMSE) are calculated between simulated and observed CO_2 at surface-insitu sites during the 1–31 January 2021 period.

station	Obs mean	Model mean			bias			rmse		
		dd_nc	dd_gr	hh_gr	dd_nc	dd_gr	hh_gr	dd_nc	dd_gr	hh_gr
bu	437.44	432.48	432.56	432.66	-4.96	-4.88	-4.78	12.09	12.1	11.94
chl	421.6	421.79	421.79	421.82	0.19	0.19	0.22	1.63	1.63	1.64
egb	426.56	428	428.01	428.08	1.44	1.45	1.53	4.37	4.41	4.35
hpb	429.72	424.08	424.06	424.13	-5.64	-5.66	-5.59	8.04	8.08	7.99
gat	430.77	426.8	426.73	426.69	-3.97	-4.04	-4.08	5.05	5.13	5.15
hnp	433.62	429.88	429.83	429.94	-3.75	-3.8	-3.68	9.4	9.33	9.4
htm	428.36	425.39	425.32	425.3	-2.97	-3.04	-3.06	3.86	3.91	3.91
ipr	437.65	424.24	424.28	424.09	-13.4	-13.37	-13.55	19.9	19.87	19.95
kre	430.32	426.42	426.39	426.31	-3.9	-3.94	-4.01	5.17	5.26	5.31
lin	432.38	428.5	428.53	428.48	-3.88	-3.85	-3.9	5.59	5.68	5.59
ryo	422.81	421.75	421.62	421.61	-1.06	-1.19	-1.2	2.14	2.2	2.2
sgp	427.51	424.83	424.83	425.01	-2.69	-2.69	-2.51	5.02	5.02	4.89
yon	422.3	420.6	420.4	420.43	-1.7	-1.9	-1.87	2.69	2.87	2.86

5 Recommendations for further model development and model optimization

5.1 Recommendations for modelling and evaluating emissions

- The use of a residential emission model (MEHNDI) coupled to the IFS urban scheme brings-mapping of urban emissions and high temporal variability associated with temperature fluctuations. This variability leads to improved variability in XCO_2 and it also presents new opportunities to run the IFS at higher resolutions than current inventories. The recommendation is to implement the MEHNDI model online in the IFS. This can be achieved by using the multiscale parameter regionalization system (Schweppe et al., 2022) that would facilitate the integration of Gamma factor maps or passing this map into the code at the script level. The CAMS-TEMPO (Guevara et al., 2021) weekly profiles could be also introduced to account for the difference in heating preferences during working and non-working days. For the modelling improvements, we recommend expanding the linear function of the emission dependency on temperature to a non-linear function in order to consider the fact that there is a limit to the increase in emissions with temperature. The other aspect that needs to be addressed further is the role of rural fuel sources such as biofuels (e.g. wood burners) in the residential heating model, which are ignored in the current implementation.
- Urban EC flux stations are becoming a relevant part of global or regional anthropogenic CO_2 emission monitoring initiatives. ICOS is currently engaging urban stations as associated stations. The ongoing project ICOS-Cities (PAUL: Pilot Applications in Urban Landscapes - Towards integrated city observatories for greenhouse gases, https://www.icos-cp.eu/projects/icos-cities) targets to develop urban GHG emission observatories, bringing together and evaluating several observation techniques. Among them, urban EC towers play a significant role in evaluating high to medium resolution emission and inversion modelling. Tall-tower EC can provide extended

footprints and therefore be more easily comparable to models. On the other hand, tall-tower measurements are more difficult to interpret and quality control due to the highly mixed signals and the decoupling of the measurements from the surface fluxes. Medium-size EC towers are more common, and the flux processing is already well-known and standardised (Feigenwinter et al., 2012). There are recent examples of how to use medium-size flux towers to evaluate or optimise high resolution emission models (Stagakis et al., 2023, Wu et al., 2022). Overall, urban EC flux observations are a valuable data source for evaluation or even optimisation of GHG emission modelling systems. Appropriate methods and standardization are still needed. However, the field is progressing fast and there are several efforts towards this direction, e.g., Ameriflux (https://ameriflux.lbl.gov),ICOS-ETC (https://www.icos-cp.eu/observations/ecosystem/etc), ICOS-Cities (https://www.icos-cp.eu/projects/icos-cities), World Meteorological Organisation (WMO, https://public.wmo.int/en).

- For the implementation of the point source database into IFS, the recommended approach is to process the emissions from the point source database directly to the IFS grid. This avoids the need to interpolate the emissions, reducing the smoothing effect at the grid scale. It also allows us to easily correct the location of any misplaced power stations, which will greatly benefit the monitoring of hotspot emissions in the CO2MVS. These two factors (interpolation and allocation of emissions) have been found to have the largest impact on CO_2 concentrations. Temporal profiles from the point source database have been found to have a smaller impact. However, we recommend re-assessing the impact of the temporal profiles using higher-resolution simulations using high-resolution satellite observations of plumes from TROPOMI and OCO_2 in 2018 to make use of additional field campaign observations, following D4.1 , Krol and van Stratum, 2021).

5.2 Recommendation for optimising emission model parameters

Process-based models simulate emissions based on parameters that can be calibrated and prognostic variables of an Earth System Model (e.g., temperature or humidity). Optimising these underlying parameters instead of the flux themselves presents several advantages: a more mechanistic approach to define the uncertainty in the emission by propagating the parameter uncertainty distribution, and the possibility to improve prognostic capabilities for the emissions.

Developments in IFS

We have identified a set of model parameters from the residential heating model in the IFS that could be optimised using the inversion framework developed in CoCO2 and described below. These are:

1. The Gamma factor in equations 2 and 3. This is currently an annual fixed country-based map with a prior estimate of annual country budgets obtained from national statistics.
2. Temperature threshold for heating in equation 1. Currently it is set to 15.5 ^{o}C at every grid point. This could be improved by estimating the threshold either by latitude or grid-point to account for changes in thermal tolerance.

These parameters will be optimised with a hybrid ensemble-variational inversion system, the Bayesian Ensemble Estimation Technique for High-resolution Optimization and Verification of Emissions of Nations (BEETHOVEN), which is currently being implemented in the IFS. This system will have the capability to optimise parameters of a process-based emission model by combining flux increments obtained from the IFS 4D-Var with a sampling estimate of the covariance matrix between the model parameters and the emissions. A schematic of the

approach is shown in Fig. 19. This method offers great flexibility, since the parameters estimation is done in an offline manner (i.e., outside and after each 4D-Var cycle), enabling the use of a variety of models in an efficient and non-intrusive way.

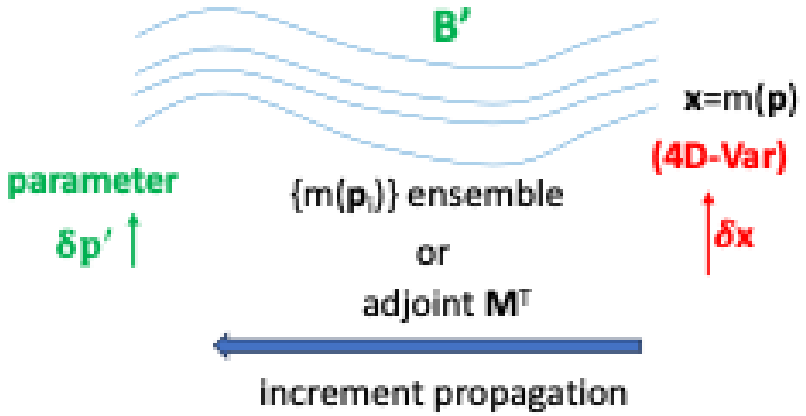

Figure 19 Schematic of the parameter optimisation method. An ensemble of model simulations (m(pi),i=1,..,k)) is used to generate the sample covariance matrix (B) between the parameters (p) and the IFS 4D-Var optimised variables (x). The resulting B matrix is then used to propagate the 4D-Var increment (dx) to the parameter space, which produces the parameter increment (dp).

Developments in FFDAS

The Fossil Fuel Data Assimilation System (Rayner et al., 2010) combines a range of potentially diverse data streams with a model of fossil fuel emissions in a variational assimilation framework. FFDAS derives a calibrated version of the fossil fuel emissions model and gridded emission fields with uncertainty ranges.

In CoCO2 WP2, the potential of using FFDAS for monitoring anthropogenic emissions has been explored. FFDAS provides a fossil fuel emission model for 4 sectors. These sectors are electricity generation, residential combustion, road transport, and the complement of these three sectors. Further sectors are being added within the CORSO project. To allow efficient calibration of the model in a variational assimilation procedure D2.5 further provides tangent and adjoint codes. The model can be operated on an arbitrary grid at the global or regional scale. For example, one could use finer resolution for specific regions/countries.

There are two principal ways of integrating the FFDAS into the global CO2MVS, which we term offline and online integration. The offline integration would be implemented as a preprocessing step that first calibrates the FFDAS against a range of data streams and then produces a sectoral fossil fuel emission field that can serve as a prior to an atmospheric transport inversion, which has surface emissions as control vector. The online integration would couple the fossil fuel emission model and a natural flux model with the atmospheric transport component and calibrate the coupled model against a combination of data streams. This combination consists of the data streams used for the calibration of FFDAS alone, additional data streams that are simulated from the natural flux component and atmospheric data streams that show the combined signal from fossil emissions and natural fluxes and thus act as a simultaneous constraint on both components. Demonstrations of the online integration are provided by Kaminski et al. (2022), CoCO2 (2023) as well as CoCO2 deliverables D6.4 (Chevalier et al., 2022a), D6.5 (Chevallier et al., 2022b), and D6.6 (Chevallier et al., 2022c) on the global scale and by Kaminski et al. (2022a) for the regional domain. A particular advantage of the online integration is that it avoids the complexities associated with passing (some approximation of) a probability density function in the high-dimensional flux space that

constitutes the interface between fossil fuel and transport models which is inherent to the offline integration. We thus recommend online integration in an operational system.

6 Conclusion

In this deliverable, we focus on improving the representation of emissions from power stations and the residential heating sector in urban locations which are two of the important emission hotspots that the CO2MVS aims to monitor. This section provides a summary of the main findings and recommendations from this deliverable, including the potential impact of the results on the future CO2MVS:

- The online simulation of CO_2 emissions from residential heating allows the representation of very high spatial and temporal resolution of the emissions from urban areas. The use of the MEHNDI residential heating model leads to an improved temporal variability of emissions, which arises from synoptic scale temperature changes. The residential heating emissions from MEHNDI have also been used in the CoCO2 nature runs v2.
- Evaluation of emissions using urban eddy covariance observations is very important and future evaluation efforts in CO2MVS should consider more sites. In Europe, ICOS observations (https://www.icos-cp.eu/observations/carbon-portal) are key to the development of a greenhouse emission verification capacity. Considering more sites will allow us to better quantify carbon emissions and sinks over given areas, and inform societies about the effects of climate change mitigation strategies. In addition, the ICOS-Cities project (https://www.icos-cp.eu/projects/icos-cities) will contribute to developing and linking urban-surface models to better monitor emissions in cities with the development of city-scale greenhouse gas observatories. The use of CoCO2 PS emissions directly on the Gaussian grid leads to a better representation of point source emission strength as well as location. It is important not to use interpolation to map the point source emissions in order to avoid smoothing errors, and this interpolation is inevitable when using gridded inventories instead of point source datasets. The impact of interpolation errors at given location - even using a mass conserving interpolation scheme - can be of the order up to 30% when using the Tco399 grid. However, at Tco1279 (~9 km), the error could be up to 110% .
- The impact of emission changes tends to be very local due to the nature of the anthropogenic fossil fuel emissions (e.g., point sources or urban heating). In this deliverable, we have performed atmospheric simulations at 25 km resolution, and we found the impact of changing the temporal profiles to be relatively small. Future work will include higher resolution simulations to enhance the emission strength and the resulting atmospheric signal around the emission hotpots using case studies with observations from satellites and field campaigns.

7 References

Agustí-Panareda, A., Barré, J., Massart, S., Inness, A., Aben, I., Ades, M., et al. (2022). The CAMS greenhouse gas reanalysis from 2003 to 2020 (pp. 1–51). EGUsphere. https://doi.org/10.5194/egusphere-2022-283

Agustí-Panareda, A., Diamantakis, M., Massart, S., Chevallier, F., Muñoz-Sabater, J., Barré, J., et al. (2019). Modelling CO2 weather – Why horizontal resolution matters. Atmospheric Chemistry and Physics, 19(11), 7347–7376. https://doi.org/10.5194/acp-19-7347-2019

Aubinet, M., Vesala, T., Papale, D., & Aubinet, M., Vesala, T., Papale, D. (2012). Eddy Covariance: A Practical Guide to Measurement and Data Analysis, Publisher: Springer, Published: 18 January 2012, https://doi.org/10.1007/978-94-007-2351-1

Batchvarova, E., & Gryning, S. E. (1991). Applied model for the growth of the daytime mixed layer. Boundary-Layer Meteorology, 56(3), 261–274. https://doi.org/10.1007/BF00120423

Buchhorn, M., Smets, B., Bertels, L., De Roo, B., Lesiv, M., Tsendbazar, N. E., et al. (2020). Copernicus global land service: Land cover 100m: Collection 3: Epoch 2019: Globe. (Version V3. 0.1) [Dataset]. Zenodo. https://doi.org/10.5281/zenodo.3939050

Boussetta, S., Balsamo, G., Beljaars, A., Panareda, A. A., Calvet, J. C., Jacobs, C., et al. (2013). Natural land carbon dioxide exchanges in the ECMWF integrated forecasting system: Implementation & offline validation. Journal of Geophysical Research: Atmospheres, 118(12), 5923–5946. https://doi.org/10.1002/jgrd.50488

Chevallier, F., Bousserez, N., Kaminski, T., Broquet, G., Fortems-Cheiney, A., Remaud, M., Santaren, D., Scholze, M., Cantarello, L., Knorr, W., Rayner, P., Voßbeck, M.:, (2022a) D6.4 Functional Requirements Specification, CoCO2 deliverable, https://coco2-project.eu/sites/default/files/2023-04/CoCO2-D6-4-V1-1.pdf

Chevallier, F., N. Bousserez, T. Kaminski, D. Brunner, G. Broquet, A. Fortems-Cheiney, M. Remaud, D. Santaren, M. Scholze, L. Cantarello, and R. Engelen (2022b), D6.5 Emission estimates for year 2021, CoCO2 deliverable, https://coco2-project.eu/sites/default/files/2023-04/CoCO2-D6-5-V1-0.pdf

Chevallier, F., Bousserez, N., Kaminski, T., Broquet, G., Fortems-Cheiney, A., Remaud, M., Santaren, D., Scholze, M., Cantarello, L., Knorr, W., Rayner, P., Voßbeck, M. (2022c): D6.6 Fitness for Purpose, CoCO2 deliverable, https://coco2-project.eu/sites/default/files/2023-04/CoCO2-D6-6-V1-1.pdf

Crawford, B., & Christen, A. (2015). Spatial source attribution of measured urban eddy covariance CO2 fluxes. Theoretical and Applied Climatology, 119(3–4), 733–755. https://doi.org/10.1007/s00704-014-1124-0

Crawford, Ben, Grimmond, C. S. B., & Christen, A. (2011). Five years of carbon dioxide fluxes measurements in a highly vegetated suburban area. Atmospheric Environment, 45(4), 896–905. https://doi.org/10.1016/j.atmosenv.2010.11.017

CoCO2 (2023). Submission of information to the 1st global stocktake: Data products from prototype systems of the eu-funded coco2 project, https://unfccc.int/documents/626619, .

Corbane, C., Sabo, F., Politis, P., & Vasileos, S. (2020). GHS-BUILT-S2 R2020A: Built-up grid derived from Sentinel-2 global image composite for reference year 2018 using convolutional neural networks (GHS-S2Net). European Commission, Joint Research Centre (JRC). https://doi.org/10.2905/016D1A34-B184-42DC-B586-E10B915DD863

De Maziere, M., Sha, M. K., Desmet, F., Hermans, C., Scolas, F., Kumps, N., et al. (2014). TCCON data from Reunion Island (RE), Release GGG2014R0. TCCON data archive, hosted by CaltechDATA. https://doi.org/10.14291/tccon.ggg2014.reunion01.R0/1149288

Denier van der Gon, H. A. C., Hendriks, C., Kuenen, J., Segers, A., & Visschedijk, A. (2011). Description of current temporal emission patterns and sensitivity of predicted AQ for temporal emission patterns, EU FP7 MACC Deliverable Rep. D_D-EMIS_1.3, TNO

Faroux, S., Kaptué Tchuenté, A. T., Roujean, J.-L., Masson, V., Martin, E., & Le Moigne, P. (2013). ECOCLIMAP-II/Europe: A twofold database of ecosystems and surface parameters at 1 km resolution based on satellite information for use in land surface, meteorological and climate models. Geoscientific Model Development, 6(2), 563–582. https://doi.org/10.5194/gmd-6-563-2013

Feigenwinter, C., Vogt, R., & Christen, A. (2012). Eddy Covariance Measurements Over Urban Areas. In Eddy Covariance (pp. 377–397). Springer Netherlands. https://doi.org/10.1007/978-94-007-2351-1_16

Granier, C., Darras, S., Denier van der Gon, H., Doubalova, J., Elguindi, N., Galle, B., et al. (2019). The Copernicus atmosphere monitoring service global and regional emissions (April 2019 version). Copernicus Atmosphere Monitoring Service. https://doi.org/10.24380/D0BN-KX16

GRTgaz (2022). Smart GRTgaz consumption data. Retrieved from https://www.smart.grtgaz.com/

Guevara, M., Jorba, O., Tena, C., Denier van der Gon, H., Kuenen, J., Elguindi, N., et al. (2021). Copernicus atmosphere monitoring service TEMPOral profiles (CAMS-TEMPO): Global and European emission temporal profile maps for atmospheric chemistry modelling. Earth System Science Data, 13(2), 367–404. https://doi.org/10.5194/essd-13-367-2021

Guevara, M., Enciso, S., Tena, C., Jorba, O., Dellaert, S., Denier van der Gon, H., and Pérez García-Pando, C. (2023): A global catalogue of CO_2 emissions and co-emitted species from power plants at a very high spatial and temporal resolution, Earth Syst. Sci. Data Discuss. [preprint], https://doi.org/10.5194/essd-2023-95, in review,.

Hase, F., Blumenstock, T., Dohe, S., Gross, J., & Kiel, M. (2014). TCCON data from Karlsruhe (DE), Release GGG2014R0. TCCON data archive, hosted by CaltechDATA. https://doi.org/10.14291/tccon.ggg2014.karlsruhe01.R0/1149270

M. Heimann, G. Esser, A. Haxeltine, J. Kaduk, D. W. Kicklighter, W. Knorr, G. H. Kohlmaier, A. D. McGuire, J. Melillo, B. Moore III, R. D. Otto, I. C. Prentice, W. Sauf, A. Schloss, S. Sitch, U. Wittenberg, G. Würth (1998), Evaluation of terrestrial carbon cycle models through simulations of the seasonal cycle of atmospheric CO2: First results of a model intercomparison study, Global Biogeochem. Cycles, 12(1), 1–24, doi:10.1029/97GB01936.

Janssens-Maenhout, G., Pinty, B., Dowell, M., Zunker, H., Andersson, E., Balsamo, G., Bézy, J.-L., Brunhes, T., Bösch, H., Bojkov, B., Brunner, D., Buchwitz, M., Crisp, D., Ciais, P., Counet, P., Dee, D., Denier van der Gon, H., Dolman, H., Drinkwater, M., Dubovik, O., Engelen, R., Fehr, T., Fernandez, V., Heimann, M., Holmlund, K., Houweling, S., Husband, R., Juvyns, O., Kentarchos, A., Landgraf, J., Lang, R., Löscher, A., Marshall, J., Meijer, Y., Nakajima, M., Palmer, P., Peylin, P., Rayner, P., Scholze, M., Sierk, B., Tamminen, J., and Veefkind, P. (2020): Towards an operational anthropogenic CO_2 emissions monitoring and verification support capacity, B. Am. Meteorol. Soc., 101, E1439–E1451, https://doi.org/10.1175/BAMS-D-19-0017.1,

Kaminski, T., Scholze, M., Rayner, P., Voßbeck, M., Buchwitz, M., Reuter, M., Knorr, W., Chen, H., Agustı-Panareda, A., Löscher, A., Meijer, Y (2022).: Assimilation of atmospheric CO2 observations from space can support national CO2 emission inventories. Environmental Research Letters, 17(1):014015, jan 2022. (doi:10.1088/1748-9326/ac3cea)

Kaminski, T., M. Scholze, P. Rayner, S. Houweling, M. Voßbeck, l, J. Silver, S. Lama, M. Buchwitz, M. Reuter, W. Knorr, H. W. Chen, G. Kuhlmann, D. Brunner, S. Dellaert, H. Denier van der Gon, I. Super. A. Löscher, and Y. Meijer (2022a). Assessing the impact of atmospheric

co2 and no2 measurements from space on estimating city-scale fossil fuel co2 emissions in a data assimilation system. Frontiers in Remote Sensing, 3,. (doi:10.3389/frsen.2022.887456)

Kawakami, S., Ohyama, H., Arai, K., Okumura, H., Taura, C., Fukamachi, T., & Sakashita, M. (2014). TCCON data from Saga (JP), Release GGG2014R0. TCCON data archive, hosted by CaltechDATA. https://doi.org/10.14291/tccon.ggg2014.saga01.R0/1149283

Kljun, N., Calanca, P., Rotach, M. W., & Schmid, H. P. (2015). A simple two-dimensional parameterisation for Flux Footprint Prediction (FFP). Geoscientific Model Development, 8(11), 3695–3713. https://doi.org/10.5194/gmd-8-3695-2015

Krol, M, van Stratum, B. (2021) D4.1 Definition of simulation cases and model system for building a library of plumes, https://www.coco2-project.eu/sites/default/files/2021-07/CoCO2-D4.1-V1-0.pdf

Lian, J., Bréon, F.-M., Broquet, G., Lauvaux, T., Zheng, B., Ramonet, M., Xueref-Remy, I., Kotthaus, S., Haeffelin, M., and Ciais, P. (2021): Sensitivity to the sources of uncertainties in the modeling of atmospheric CO_2 concentration within and in the vicinity of Paris, Atmos. Chem. Phys., 21, 10707–10726, https://doi.org/10.5194/acp-21-10707-2021,.

Lipson, M., Grimmond, S., Best, M., Chow, W. T. L., Christen, A., Chrysoulakis, N., Coutts, A., Crawford, B., Earl, S., Evans, J., Fortuniak, K., Heusinkveld, B. G., Hong, J. J.-W. W., Hong, J. J.-W. W., Järvi, L., Jo, S., Kim, Y.-H. H., Kotthaus, S., Lee, K., … Ward, H. C. (2022). Harmonized gap-filled datasets from 20 urban flux tower sites. Earth System Science Data Discussions, 14(June), 5157–5178. https://doi.org/10.5194/essd-2022-65

Massart, S., Agust.-Panareda, A., Heymann, J., Buchwitz, M., Chevallier, F., Reuter, M., et al. (2016). Ability of the 4-D-Var analysis of the GOSAT BESD XCO 2 retrievals to characterize atmospheric CO2 at large and synoptic scales. Atmospheric Chemistry and Physics, 16(3), 1653–1671. https://doi.org/10.5194/acp-16-1653-2016

Nemry, B., FrançOis, L., Gérard, J.-.-C., Bondeau, A., Heimann, M. and THE PARTICIPANTS OF THE POTSDAM NPP MODEL INTERCOMPARISON (1999), Comparing global models of terrestrial net primary productivity (NPP): analysis of the seasonal atmospheric CO2 signal. Global Change Biology, 5: 65-76. https://doi.org/10.1046/j.1365-2486.1999.00008.x

McNorton, J., Agusti-Panareda, A., Arduini, G., Balsamo, G., Bousserez, N., Boussetta, S., et al. (2023). An urban scheme for the ECMWF Integrated forecasting system: Global forecasts and residential CO2 emissions. Journal of Advances in Modeling Earth Systems, 15, e2022MS003286. https://doi. Org/10.1029/2022MS003286

McNorton, J. R., Arduini, G., Bousserez, N., Agustí-Panareda, A., Balsamo, G., Boussetta, S., et al. (2021). An urban scheme for the ECMWF integrated forecasting system: Single-column and global offline application. Journal of Advances in Modeling Earth Systems, 13, e2020MS002375. https://doi.org/10.1029/2020MS002375

McNorton, J., Bousserez, N., Agustí-Panareda, A., Balsamo, G., Cantarello, L., Engelen, R., et al. (2022). Quantification of methane emissions from hotspots and during COVID-19 using a global atmospheric inversion. Atmospheric Chemistry and Physics, 22(9), 5961–5981. https://doi.org/10.5194/acp-22-5961-2022

McNorton, J. R., Bousserez, N., Agustí-Panareda, A., Balsamo, G., Choulga, M., Dawson, A., et al. (2020). Representing model uncertainty for global atmospheric CO2 flux inversions using ECMWF-IFS-46R1. Geoscientific Model Development, 13(5), 2297–2313. https://doi.org/10.5194/gmd-13-2297-2020

Moriwaki, R., & Kanda, M. (2004). Seasonal and diurnal fluxes of radiation, heat water vapor, and carbon dioxide over a suburban area. Journal of Applied Meteorology, 43(11), 1700–1710. https://doi.org/10.1175/JAM2153.1

Nicolini, G., Antoniella, G., Carotenuto, F., Christen, A., Ciais, P., Feigenwinter, C., Gioli, B., Stagakis, S., Velasco, E., Vogt, R., Ward, H. C., Barlow, J., Chrysoulakis, N., Duce, P., Graus,

M., Helfter, C., Heusinkveld, B., Järvi, L., Karl, T., … Papale, D. (2022). Direct observations of CO2 emission reductions due to COVID-19 lockdown across European urban districts. Science of The Total Environment, 830, 154662. https://doi.org/10.1016/j.scitotenv.2022.154662

Nieuwstadt, F. T. M. (1981). The steady-state height and resistance laws of the nocturnal boundary layer: Theory compared with cabauw observations. Boundary-Layer Meteorology, 20(1), 3–17. https://doi.org/10.1007/BF00119920

Petri, C., Rousogenous, C., Warneke, T., Vrekoussis, M., Sciare, J., & Notholt, J. (2019). TCCON data from Nicosia, Cyprus (CY), release GGG2014. R0. TCCON data archive, hosted by CaltechDATA. https://doi.org/10.14291/tccon.ggg2020.nicosia01.R0

Politakos, K., Stagakis, S., Feigenwinter, C., Roth, M., & Chrysoulakis, N. (2023a). Comparison of urban eddy covariance CO2 and heat fluxes measured at two flux towers in a Mediterranean city. The 11th International Conference on Urban Climate. https://doi.org/10.13140/RG.2.2.34950.96325

Politakos, K., Stagakis, S., Feigenwinter, C., Roth, M., & Chrysoulakis, N. (2023). Dynamic changes in urban form and function affect carbon dioxide fluxes in a Mediterranean city. JURSE 2023. https://doi.org/10.13140/RG.2.2.14114.20166

Quayle, R. G., & Diaz, H. F. (1980). Heating degree day data applied to residential heating energy consumption. Journal of Applied Meteorology and Climatology, 19(3), 241–246. https://doi.org/10.1175/1520-0450(1980)019<0241: HDDDAT>2.0.CO;2

Rayner, P. J., Raupach, M. R., Paget, M., Peylin, P., and Koffi, E. (2010), A new global gridded data set of CO2 emissions from fossil fuel combustion: Methodology and evaluation, J. Geophys. Res., 115, D19306, doi:10.1029/2009JD013439.

Spinoni, J., Vogt, J., & Barbosa, P. (2015). European degree-day climatologies and trends for the period 1951–2011. International Journal of Climatology, 35(1), 25–36. https://doi.org/10.1002/joc.3959

Soulie, A., Granier, C., Darras, S., Zilbermann, N., Doumbia, T., Guevara, M., Jalkanen, J.-P., Keita, S., Liousse, C., Crippa, M., Guizzardi, D., Hoesly, R., and Smith, S.: Global Anthropogenic Emissions (CAMS-GLOB-ANT) for the Copernicus Atmosphere Monitoring Service Simulations of Air Quality Forecasts and Reanalyses, Earth Syst. Sci. Data Discuss. [preprint], https://doi.org/10.5194/essd-2023-306, in review, 2023.

Stagakis, S., Chrysoulakis, N., Spyridakis, N., Feigenwinter, C., & Vogt, R. (2019). Eddy Covariance measurements and source partitioning of CO2 emissions in an urban environment: Application for Heraklion, Greece. Atmospheric Environment, 201(August 2018), 278–292. https://doi.org/10.1016/j.atmosenv.2019.01.009

Stagakis, S., Feigenwinter, C., Vogt, R., & Kalberer, M. (2022). A High-Resolution Monitoring Approach of Urban Co2 Fluxes. Part 2 - Optimisation Framework Using Eddy Covariance Observations. SSRN Electronic Journal, 903(November 2022), 166035. https://doi.org/10.2139/ssrn.4280928

Stagakis, S., Feigenwinter, C., Vogt, R., & Kalberer, M. (2023). A high-resolution monitoring approach of urban CO2 fluxes. Part 1 - bottom-up model development. Science of the Total Environment, 858(July 2022), 160216. https://doi.org/10.1016/j.scitotenv.2022.160216

Schweppe, R., Thober, S., Müller, S., Kelbling, M., Kumar, R., Attinger, S., and Samaniego, L.: MPR 1.0: a stand-alone multiscale parameter regionalization tool for improved parameter estimation of land surface models, Geosci. Model Dev., 15, 859–882, https://doi.org/10.5194/gmd-15-859-2022, 2022. Te., Y., Jeseck, P., & Janssen, C. (2014). TCCON data from Paris (FR), Release GGG2014R0. TCCON data archive, hosted by CaltechDATA. https://doi.org/10.14291/tccon.ggg2014.paris01.R0/1149279

Wennberg, P. O., Wunch, D., Roehl, C., Blavier, J.-F., Toon, G. C., & Allen, N. (2014). TCCON

data from Caltech (US), Release GGG2014R0. TCCON data archive, hosted by CaltechDATA. https://doi.org/10.14291/tccon.ggg2014.pasadena01.R0/1149162

Wheeler, D. and Ummel, K.: Calculating CARMA: Global Estimation of CO2 Emissions from the Power Sector, available at: https://www.cgdev.org/publication/calculating-carmaglobal-estimation-co2- emissions-power-sector-working-paper145 (last access: February 2023), 2008.

Wunch, D., Toon, G. C., Blavier, J. F. L., Washenfelder, R. A., Notholt, J., Connor, B. J., et al. (2011). The total carbon column observing network. Philosophical Transactions of the Royal Society A: Mathematical, Physical & Engineering Sciences, 369(1943), 2087–2112. https://doi.org/https://doi.org/10.1098/rsta.2010.024010.1098/rsta.2010.0240

Zilitinkevich, S. S., Tyuryakov, S. A., Troitskaya, Y. I., & Mareev, E. A. (2012). Theoretical models of the height of the atmospheric boundary layer and turbulent entrainment at its upper boundary. Izvestiya - Atmospheric and Ocean Physics, 48(1), 133–142. https://doi.org/10.1134/S0001433812010148

8 Supplementary Material

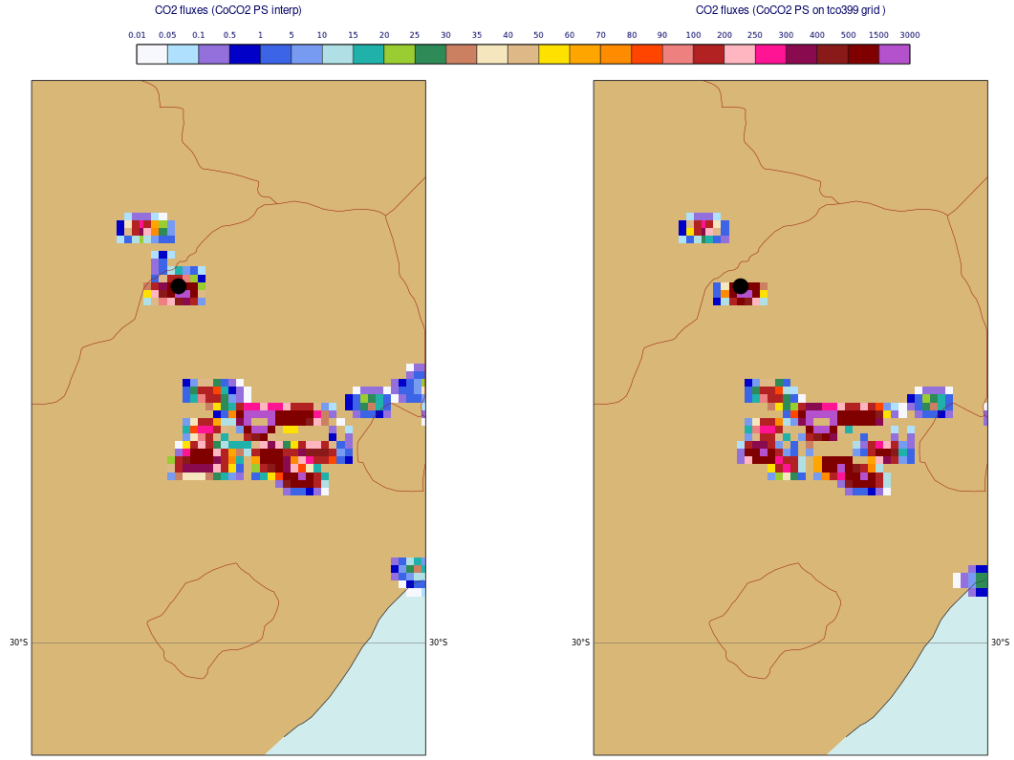

Figure S 1 January 2021 total CO2 emissions [g/m2] from power plants in South Africa, near Matimba from CoCO2 PS inventory remapped from regular grid on the Tco399 grid (left panel) and directly on the Tco399 grid (right panel). The black dot represents the location of Matimba.

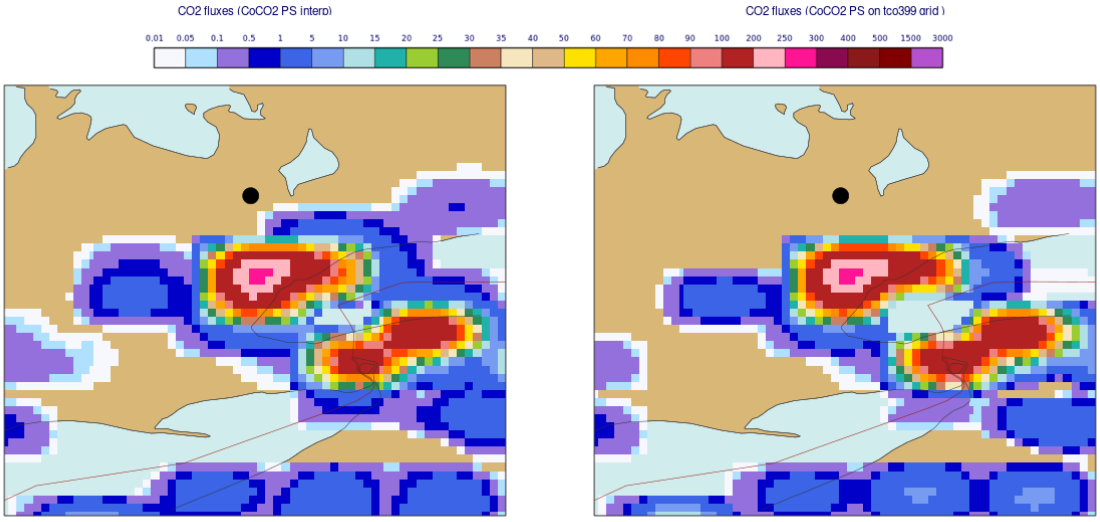

Figure S 2 January 2021 total CO2 emissions [g/m2] from power plants near Egbert, ON, Canada from CoCO2 PS inventory remapped from the regular grid on the Tco399 grid (left panel) and directly on the Tco399 grid (right panel). The black dot represents the location of Egbert

Document History

Version	Author(s)	Date	Changes
	Name (Organisation)	dd/mm/yyyy	

Internal Review History

Internal Reviewers	Date	Comments
Name (Organisation)	dd/mm/yyyy	
Elena Saltikoff and Sindu Raj Parampil	31/10/2023	Suggesting minor edits for readability and style.